

Quadrature Space-Frequency Index Modulation for Energy-Efficient 5G Wireless Communication Systems

Piya Patcharamaneepakorn, *Member, IEEE*, Cheng-Xiang Wang[✉], *Fellow, IEEE*, Yu Fu, El-Hadi M. Aggoune, *Senior Member, IEEE*, Mohammed M. Alwakeel, *Senior Member, IEEE*, Xiaofeng Tao, *Senior Member, IEEE*, and Xiaohu Ge[✉], *Senior Member, IEEE*

Abstract—This paper proposes a novel quadrature space-frequency index modulation (QSF-IM) scheme as a promising energy-efficient radio-access technology for the fifth generation (5G) wireless systems. Motivated by the potential energy saving of spatial modulation (SM) with the part of information being carried through antenna indexes, the proposed scheme further leverages the benefits of SM by applying the idea across the spatial and frequency domains. Moreover, by deploying dual antenna constellation for in-phase and quadrature-phase transmission, the proposed scheme can enhance data rate at no extra cost of energy consumption, leading to further improvement in energy efficiency. Theoretical bit error rate and achievable sum-rate of the proposed scheme over frequency-selective correlated Rician and Rayleigh fading channels are derived and are shown to have good agreement with simulations. Furthermore, the effectiveness of the proposed scheme is analyzed through a comprehensive list of performance metrics, including spectral efficiency (SE), energy efficiency (EE), cost efficiency (CE), and economic efficiency. Performance trade-offs between these metrics are thoroughly investigated. Compared with other existing schemes, the proposed QSF-IM scheme is demonstrated to offer better EE-SE and EE-CE tradeoffs, and can therefore be considered as a potential candidate for energy-spectral efficient 5G systems.

Index Terms—Quadrature spatial modulation, index modulation, spectral efficiency, energy efficiency, cost efficiency, economic efficiency.

I. INTRODUCTION

THE fifth generation (5G) wireless system is targeted to offer 1000 times the system capacity, 10 times the spectral efficiency (SE) and data rate, and 25 times the average cell throughput, compared to the fourth generation (4G) network [1]. Not only does the 5G network aim to enhance system throughput and user data rate, significant improvement in energy efficiency (EE) and cost efficiency (CE) is also expected [2]. This has attracted considerable interest in researching revolutionary wireless technologies to meet these challenging targets.

Multiple-input multiple-output (MIMO) technology is one of the key techniques to improve the system capacity and reliability of wireless communication networks [3]–[6]. Various MIMO techniques have been intensively investigated in the literature, including spatial multiplexing, spatial diversity and beamforming schemes [4], [5]. In 2008, another MIMO transmission scheme, referred to spatial modulation (SM) [7]–[10], was proposed and is envisioned to be a promising alternative candidate for 5G radio access technology [1], [10]. In SM systems, user data is conveyed by two information carrying units, namely the antenna index and the modulated symbol. Furthermore, only a single transmit antenna is active at each time instant [7]. Consequently, only one radio frequency (RF) chain is required at the transmitter, leading to significant advantages over the conventional MIMO schemes, including mitigation of inter-channel interference, relaxation of inter-antenna synchronization requirements, and reduction of receiver complexity [9].

SM has been further enhanced into variant schemes. A special form of SM, when the user information is carried by the antenna indexes only, was investigated in [11] and [12] and is referred as the space-shift keying (SSK) scheme. Generalized spatial modulation (Gen-SM) and generalized SSK (GSSK) techniques, allowing transmission on multiple active antennas, were studied in [13]–[15]. Moreover, instead of using the indexes of the transmit antennas, the indexes of the receive antennas were adopted for carrying information

Manuscript received May 12, 2017; revised October 9, 2017; accepted November 13, 2017. Date of publication November 23, 2017; date of current version July 13, 2018. This work was supported by the EU H2020 ITN 5G Wireless project (Grant No. 641985), EU H2020 RISE TESTBED project (Grant No. 734325), EU FP7 QUICK project (Grant No. PIRSES-GA-2013-612652), EPSRC TOUCAN project (Grant No. EP/L020009/1), Natural Science Foundation of China (Grant No. 61210002), the SNCS Research Center, University of Tabuk, Saudi Arabia, and the China International Joint Research Center of Green Communications and Networking (No. 2015B01008). The associate editor coordinating the review of this paper and approving it for publication was J. Choi. (*Corresponding author: Cheng-Xiang Wang.*)

P. Patcharamaneepakorn was with the School of Engineering and Physical Sciences, Institute of Sensors, Signals and Systems, Heriot-Watt University, Edinburgh EH14 4AS, U.K. He is now with True Corporation, Bangkok 10310, Thailand (e-mail: piya_pat@truecorp.co.th).

C.-X. Wang and Y. Fu are with the School of Engineering and Physical Sciences, Institute of Sensors, Signals and Systems, Heriot-Watt University, Edinburgh EH14 4AS, U.K. (e-mail: cheng-xiang.wang@hw.ac.uk; y.fu@hw.ac.uk).

E.-H. M. Aggoune and M. M. Alwakeel are with the Sensor Networks and Cellular Systems Research Center, University of Tabuk, Tabuk 47315/4031, Saudi Arabia (e-mail: haggoune.snrc@ut.edu.sa; alwakeel@ut.edu.sa).

X. Tao is with the Wireless Technology Innovation Institute, Beijing University of Posts and Telecommunications, Beijing 100876, China (e-mail: taoxf@bupt.edu.cn).

X. Ge is with the School of Electronic Information and Communications, Huazhong University of Science and Technology, Wuhan 430074, China (e-mail: xhge@mail.hust.edu.cn).

Color versions of one or more of the figures in this paper are available online at <http://ieeexplore.ieee.org>.

Digital Object Identifier 10.1109/TCOMM.2017.2776956

bits, resulting in the receive SM (RSM) or precoding-aided SM (PSM) schemes [16], [17]. In addition to the spatial domain, the concept of index modulation (IM) can also be applied across other domains, including the time and frequency domains, leading to space-time shift keying (STSK) [18] and orthogonal frequency division multiplexing with index modulation (OFDM-IM) [19]–[23] techniques, respectively. Other schemes that combine OFDM-IM and MIMO transmission techniques, referred to as MIMO OFDM with index modulation (MIMO-OFDM-IM) schemes, are also presented in [24]–[26]. Furthermore, an enhanced SSK scheme that utilizes dual antenna constellation was proposed in [27] and is referred to as Bi-SSK (Bi-SSK) modulation. By splitting the real part and the imaginary part of the SSK symbols and transmitting them onto separate antenna constellations, double spectral efficiency can be achieved with comparable receiver complexity with the conventional SSK scheme. This idea was generalized in [28] and [29] for supporting arbitrary signal modulation, and is known as the quadrature spatial modulation (QSM) scheme. It should be noted that, although dual antenna constellation is deployed, Bi-SSK and QSM techniques rely on a single active modulated symbol as well as exploit the antenna constellation on the spatial domain only.

Motivated by Bi-SSK and QSM techniques, this paper proposes a novel SM-based transmission scheme that enables the application of dual antenna constellation to arbitrary numbers of active modulated symbols and can be applied across spatial and frequency domains. The proposed scheme is referred to as a *quadrature space-frequency index modulation (QSF-IM)* scheme. Bit error rate (BER) performance and SE of the proposed scheme are analyzed and are demonstrated to be in close proximity to simulation. Other performance metrics, including EE, CE, and economic efficiency (ECE), are also investigated. The proposed scheme is shown to outperform the existing and conventional SM-based schemes in terms of BER and SE performance, and offer better performance trade-offs with respect to SE-EE, SE-CE (or SE-ECE), and EE-CE (or EE-ECE). The key contributions of this paper can be summarized as follows:

- 1) A novel SM-based transmission scheme, namely the QSF-IM scheme, is proposed and is studied with maximum likelihood (ML) detection. In contrast to [27]–[29], the proposed scheme allows the use of dual antenna constellation with multiple active modulated symbols. Moreover, the dual antenna constellation is not only utilized in the spatial domain, but also applied across the frequency domain, forming a joint space-frequency (SF) resource unit, referred to as a SF resource block (RB), which is suitable for deployment in 5G wireless systems.
- 2) BER performance and SE of the proposed scheme over frequency-selective and correlated Rician (and Rayleigh) fading channels are derived and are shown to agree well with simulations. To the best of the authors' knowledge, this is the first analytical result for dual antenna constellation-based SM schemes over frequency-selective and correlated Rician fading channels.

- 3) This paper is also one of the pioneering works that comprehensively incorporate various metrics into performance evaluation. Not only are BER and SE considered in this work, EE, CE, and ECE are also studied. Trade-offs between these metrics, such as SE-EE, SE-CE (or SE-ECE), and EE-CE (or EE-ECE) trade-offs, are thoroughly analyzed. In particular, the proposed scheme is demonstrated to achieve the better SE-EE and EE-CE trade-offs, compared with existing schemes, highlighting the potential of its deployment in energy-efficient 5G networks.

The remainder of the paper is organized as follows. In Section II, the system model and the proposed QSF-IM scheme are introduced. In Section III, the BER analysis of the proposed QSF-IM scheme is described. The ergodic achievable rate is studied in Section IV. In Section V, EE, SE CE, and ECE are analyzed. Simulation results are presented in Section VI. Finally, conclusions are drawn in Section VII.

Notation: $\text{Tr}(\cdot)$, $(\cdot)^T$, and $(\cdot)^H$ denote the trace, transpose, and Hermitian, operations, respectively. $C(m, n)$ denotes the binomial coefficient and $[\mathbf{A}]_{u,v}$ represents the (u, v) -th element of matrix \mathbf{A} . The vectorization, $\text{vec}(\mathbf{A})$, is the operator which stacks the columns of \mathbf{A} into a column vector, and $\text{ivec}(\mathbf{a}, r, c)$ is defined as the operator that arranges a column vector \mathbf{a} into a matrix with r rows and c columns. An $n \times 1$ vector with all elements being 1 is also denoted as $\mathbf{1}_n$. The block diagonalization operation of square matrices is denoted as $\text{blkdiag}\{\cdot\}$. Moreover, $\mathbf{A}_G^{\mathcal{F}}$ or $(\mathbf{A})_G^{\mathcal{F}}$ represent submatrices of the $r \times c$ matrix \mathbf{A} , formed by taking only the rows indexed by $\mathcal{F} \subseteq \{1, 2, \dots, r\}$ and columns indexed by $G \subseteq \{1, 2, \dots, c\}$, and $\{\alpha_{n,m}\}$ denotes the set of all $C(m, n)$ ordered length- n subsets of the numbers $\{1, 2, \dots, m\}$.

II. SYSTEM MODEL AND THE PROPOSED QSF-IM SCHEME

Let us consider a MIMO-orthogonal frequency division multiplexing (OFDM) system over a correlated frequency-selective Rician fading channel with N_t transmit antennas and N_r receive antennas. The number of OFDM subcarriers and the size of fast Fourier transform (FFT) are assumed to be N . The total number of N subcarriers is divided into n_g groups, each with n subcarriers, i.e., $n_g = \frac{N}{n}$. The n subcarriers for each group with N_t transmit antennas form a RB, containing nN_t SF resource units.

A. The Proposed QSF-IM Transmission Scheme

The block diagram of the proposed QSF-IM transmitter can be depicted in Fig. 1. For each RB, a block of m information bits are processed and divided into three groups, i.e., $m = m_1 + m_2 + m_3$. The first group with $m_1 = k \log_2(M)$ bits is mapped into k modulated symbols by M -ary quadrature amplitude modulation (QAM), phase shift keying (PSK), or other symbol modulation schemes. Each modulated symbol is assumed to have unit average power. The resulting k modulated symbols are then decomposed into their real and imaginary parts, corresponding to the

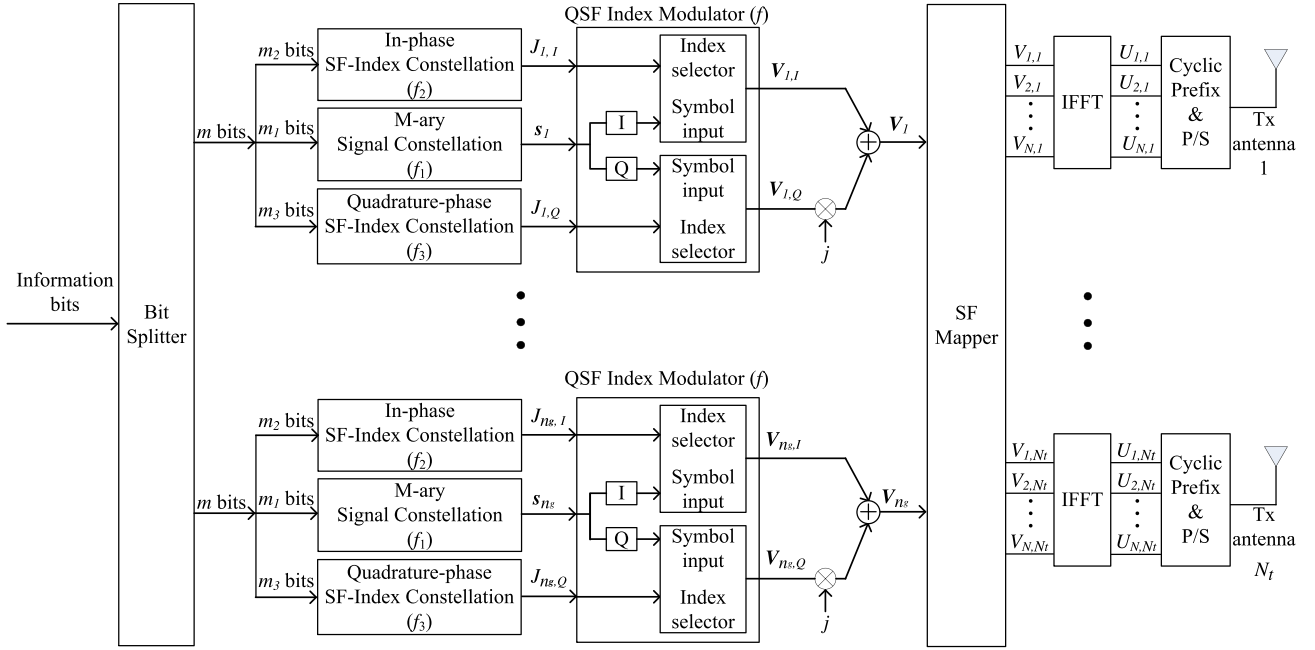


Fig. 1. Block diagram of the proposed QSF-IM transmitter.

in-phase and the *quadrature-phase* components of the modulated signal, respectively. The k in-phase components are further mapped into k out of nN_t available SF indexes in the RB using the information bits of the second group with $m_2 = \lfloor \log_2[C(nN_t, k)] \rfloor$ bits. This process can be referred to as *space-frequency index modulation (SF-IM)*. A similar process is applied to the k quadrature-phase components using the third group with $m_3 = \lfloor \log_2[C(nN_t, k)] \rfloor$ information bits. The in-phase and quadrature-phase components are then combined and processed by the antenna-subcarrier mapper before conventional OFDM signal processing in each transmit antenna chain.

Let us consider a block of information bits of the b -th RB, denoted as $\mathbf{d}_b = [\mathbf{d}_{b,1}^T, \mathbf{d}_{b,2}^T, \mathbf{d}_{b,3}^T]^T$ with $\mathbf{d}_{b,i}^T \in \mathbb{I}^{m_i}$, $i \in \{1, 2, 3\}$ and $\mathbb{I} \in \{0, 1\}$. Let $f_1 : \mathbf{d}_{b,1} \rightarrow \mathbf{s}_b$ represent a mapping from $\mathbf{d}_{b,1}$ to a vector of modulated symbols, denoted as $\mathbf{s}_b \in \mathbb{S}^k$ with \mathbb{S} being a set of M constellation symbols and $\mathbb{E}\{\mathbf{s}_b \mathbf{s}_b^H\} = E_s \mathbf{I}_k$. The SF-IM process for in-phase and quadrature components can also be defined as $f_2 : \mathbf{d}_{b,2} \rightarrow J_{b,I}$ and $f_3 : \mathbf{d}_{b,3} \rightarrow J_{b,Q}$, respectively, with $J_{b,I}$ (and $J_{b,Q}$) being a set of k active SF resource units associated to the in-phase (quadrature-phase) signal. Specifically, $J_{b,q} = \{j_{b,q,1}, j_{b,q,2}, \dots, j_{b,q,k}\}$ for $q \in \{I, Q\}$, with the active index of the i -th symbol given by $j_{b,q,i} = (c_i - 1)N_t + a_i$, with $a_i \in \{1, \dots, N_t\}$ and $c_i \in \{1, \dots, n\}$, corresponding to the a -th transmit antenna and the relative subcarrier index c_i of the b -th RB. Note that the absolute subcarrier index in the OFDM block for the subcarrier index c_i in the b -th RB can be given as $(b-1)n + c_i$, with $1 \leq (b-1)n + c_i \leq N$. Denoting $J_b = (J_{b,I}, J_{b,Q})$ as the spatial constellation symbols, the constellation size of J_b can be given by $M_J = 2^{m_2 + m_3}$. With the modulated symbols, \mathbf{s}_b , and the spatial constellation symbols, J_b , the transmitted symbols of the b -th RB in the frequency domain can be expressed as $\mathbf{V}_b = \mathbf{V}_{b,I} + j\mathbf{V}_{b,Q}$,

where

$$(\mathbf{V}_{b,I}, \mathbf{V}_{b,Q}) = f(\mathbf{s}_b, J_b) \quad (1)$$

with $f : (\mathbf{s}_b, J_b) \rightarrow (\mathbf{V}_{b,I}, \mathbf{V}_{b,Q})$ being a mapping function from (\mathbf{s}_b, J_b) to $(\mathbf{V}_{b,I}, \mathbf{V}_{b,Q})$, and $\mathbf{V}_{b,I}, \mathbf{V}_{b,Q} \in \mathbb{C}^{n \times N_t}$ representing the in-phase and the quadrature-phase components of \mathbf{V}_b . Note that only k out of nN_t elements of $\mathbf{V}_{b,q}$ are non-zero, corresponding to $J_{b,q}$. The transmit symbols for all RBs in the frequency domain can be given by $\mathbf{V} = [\mathbf{V}_1^T, \mathbf{V}_2^T, \dots, \mathbf{V}_{n_g}^T]^T \in \mathbb{C}^{n \times N_t}$. After processed by the inverse FFT (IFFT), the time-domain OFDM block can be expressed as

$$\mathbf{U} = \frac{1}{\sqrt{N}} \mathbf{W}_N^H \mathbf{V} \quad (2)$$

where \mathbf{W}_N is the discrete Fourier transform (DFT) matrix, i.e., $[\mathbf{W}_N]_{u,v} = e^{-j\frac{2\pi uv}{N}}$ with $\frac{1}{N} \mathbf{W}_N^H \mathbf{W}_N = \mathbf{I}_N$. It follows that $\mathbb{E}\{\text{Tr}(\mathbf{U}^H \mathbf{U})\} = n_g k E_s$. A cyclic prefix (CP) of length N_{cp} samples is then appended to the beginning of the OFDM block. The OFDM signal in the time-domain is obtained after parallel-to-serial (P/S) and digital-to-analog RF conversion. Note that the total transmitted energy per OFDM block can be written as $\left(\frac{N+N_{cp}}{N}\right) n_g k E_s = (N+N_{cp}) \left(\frac{k}{n}\right) E_s$ and the energy per bit (E_b) is given by $\left(\frac{N+N_{cp}}{N}\right) \left(\frac{n_g k E_s}{n_g m}\right) = \left(\frac{N+N_{cp}}{N}\right) \left(\frac{k}{m}\right) E_s$.

B. System Model

Referring to the equivalent channel matrix of the b -th RB in the frequency domain, $\mathbf{G}_b \in \mathbb{C}^{nN_t \times nN_t}$, as given in (54) in Appendix A, the equivalent frequency-domain representation of the system can be expressed as

$$\mathbf{y}_b = \sqrt{E_s} \mathbf{G}_b \mathbf{x}_b + \mathbf{w}_b \quad (3)$$

where $\mathbf{y}_b \in \mathbb{C}^{nN_r}$ and $\mathbf{w}_b \in \mathbb{C}^{nN_r}$ are the received signal vector and the noise vector in the frequency domain, respectively, and the normalized transmitted vector \mathbf{x}_b can be obtained as

$$\mathbf{x}_b = \frac{1}{\sqrt{E_s}} \text{vec} \left(\mathbf{V}_b^T \right) = [\mathbf{x}_b(1)^T, \dots, \mathbf{x}_b(n)^T]^T \quad (4)$$

with $\mathbf{x}_b(c) \in \mathbb{C}^{N_t}$ is the transmitted vector of the c -th subcarrier in the b -th RB. Each element of \mathbf{w}_b is assumed to be independent and identically distributed (i.i.d.) complex Gaussian random variable with zero mean and variance N_0 . It is also useful in subsequent discussion to express (3) in an alternative form, as given by

$$\mathbf{y}_b = \sqrt{E_s} \mathbf{X}_b \mathbf{g}_b + \mathbf{w}_b \quad (5)$$

where $\mathbf{g}_b = \text{vec}(\mathbf{G}_b^T)$ and $\mathbf{X} = \text{blkdiag}\{\mathbf{X}_b(c)\}$ with $c \in \{1, \dots, n\}$
 $\mathbf{X}_b(c) = \mathbf{I}_{N_r} \otimes \mathbf{x}_b(c)^T$.

C. Signal Detection

At the receiver, the active SF indexes and the transmitted modulated symbols need to be detected for each RB. Denoting $\mathbf{x}_b = (\mathbf{x}_{b,I} + j\mathbf{x}_{b,Q})$ with $\mathbf{x}_{b,I}$, $\mathbf{x}_{b,Q}$ being the in-phase and the quadrature-phase components of \mathbf{x}_b , the ML detection can be applied by searching for all of 2^m possible combinations of $\mathbf{x}_{b,I}$, $\mathbf{x}_{b,Q}$, as given by

$$[\hat{\mathbf{x}}_{b,I}, \hat{\mathbf{x}}_{b,Q}] = \arg \min_{\{\mathbf{x}_{b,I}, \mathbf{x}_{b,Q}\}} \|\mathbf{y}_b - \sqrt{E_s} \mathbf{G}_b (\mathbf{x}_{b,I} + j\mathbf{x}_{b,Q})\|^2. \quad (6)$$

Consequently, the detected signal vectors $\hat{\mathbf{x}}_{b,I}$, $\hat{\mathbf{x}}_{b,Q}$ can be used to retrieve the signal constellation and the spatial constellation symbols, (\hat{s}_b, \hat{j}_b) , as well as the estimated information bits, $\hat{\mathbf{d}}_b$. It is noted that the ML detector in (6) is assumed in the performance analysis in Section III. Nevertheless, the decoding complexity of the ML detector is in the order of $\mathcal{O}(2^m) \approx \mathcal{O}((nN_tM)^k)$ per RB, which could become impractical due to exponentially increasing complexity, especially with higher order modulation and higher MIMO order. Low-complexity near-/sub-optimal detectors should, therefore, be developed for practical deployment, e.g., by extending the works in [22] and [24]–[26]. This will be considered as one of the key aspects in our future work, as highlighted in Section VIII.

D. Special Cases of the QSF-IM Scheme

Special cases of the proposed QSF-IM can be shown to be equivalent to several existing SM-based schemes. Specifically, the QSM scheme [28], [29] is a special case of the QSF-IM scheme when QSF-IM is applied across the spatial domain only. Another special form of the QSF-IM when the information bits are conveyed by SF indexes only can be referred to as QSF-index shift keying (QSF-ISK). It can be shown that the Bi-SSK scheme [27] is a special case of QSF-ISK with QSF-ISK being adopted across the spatial domain only. Moreover, by exploiting the frequency domain only, i.e., using $N_t = 1$, QSF-IM can be reduced to a quadrature OFDM index modulation (Q-OFDM-IM) scheme. A similar scheme as Q-OFDM-IM is also

proposed in [21], wherein it is referred to as an OFDM with generalized index modulation 2 (OFDM-GIM2) scheme. Further, the OFDM-IM scheme [19] is shown to be a special case of Q-OFDM-IM when the single (instead of dual) antenna constellation is applied.

III. BER ANALYSIS OF THE QSF-IM SCHEME

In this section, the BER performance of the QSF-IM scheme is evaluated by using the well-known union bound, which can be written as

$$\text{BER} \leq \frac{1}{m_{\mathbf{X}} n_{\mathbf{X}}} \sum_{\mathbf{X}} \sum_{\hat{\mathbf{X}}} P(\mathbf{X} \rightarrow \hat{\mathbf{X}}) n_H(\mathbf{X}, \hat{\mathbf{X}}) \quad (7)$$

with $P(\mathbf{X} \rightarrow \hat{\mathbf{X}})$ denoting the pairwise error probability (PEP), i.e., the probability that the codeword \mathbf{X} is decoded as $\hat{\mathbf{X}}$ assuming that \mathbf{X} and $\hat{\mathbf{X}}$ are only two possible codewords, and $n_H(\mathbf{X}, \hat{\mathbf{X}})$ being the Hamming distance between \mathbf{X} and $\hat{\mathbf{X}}$. Moreover, $m_{\mathbf{X}}$ and $n_{\mathbf{X}}$ represent the number of information bits and the number of the possible realizations of \mathbf{X} , respectively.

A. QSF-IM With Correlated Rician Fading Channels

By extending (5) to all RBs, the equivalent frequency-domain representation of the system can be written as

$$\mathbf{y}_F = \sqrt{E_s} \mathbf{X}_F \mathbf{g}_F + \mathbf{w}_F \quad (8)$$

with $\mathbf{y}_F = [\mathbf{y}_1^T, \dots, \mathbf{y}_{n_g}^T]^T$, $\mathbf{X}_F = \text{blkdiag}\{\mathbf{X}_1, \dots, \mathbf{X}_{n_g}\}$, $\mathbf{g}_F = [\mathbf{g}_1^T, \dots, \mathbf{g}_{n_g}^T]^T$, and $\mathbf{w}_F = [\mathbf{w}_1^T, \dots, \mathbf{w}_{n_g}^T]^T$. It can be shown in Appendix B that \mathbf{g}_F is a complex Gaussian vector with the mean vector $\bar{\mathbf{g}}_F$ and the covariance matrix \mathbf{Q}_F given by (57) and (60), respectively. Following similar arguments in [19], it can be shown that \mathbf{Q}_F is a Hermitian Block-Toeplitz matrix and the BER performance for each RB is identical. Any arbitrary RB can be considered and thus, the subscript b in (3) and (5) will be omitted in subsequent discussions, without loss of generality. Considering (5), it follows from (57) and (60) that the mean vector of \mathbf{g} , denoted as $\bar{\mathbf{g}}$, can be given by

$$\bar{\mathbf{g}} = \sqrt{\frac{K}{K+1}} (\mathbf{1}_n \otimes \mathbf{I}_{N_r N_t}) \text{vec}(\bar{\mathbf{H}}(0)^T) \quad (9)$$

and the covariance matrix, denoted as \mathbf{Q} , can be expressed as

$$\mathbf{Q} = \frac{1}{K+1} (\mathbf{W}_n \check{\mathbf{\Omega}} \mathbf{W}_n^H) \otimes (\mathbf{R}_r \otimes \mathbf{R}_t) \quad (10)$$

where $\mathbf{W}_n \in \mathbb{C}^{n \times N}$ being a submatrix containing the first n rows of \mathbf{W}_N . It can be verified that the covariance matrices of other RBs, being $nN_r N_t \times nN_r N_t$ submatrices centered along the main diagonal of \mathbf{Q}_F with appropriate starting positions, are identical to \mathbf{Q} . It is known from [19] that the conditional pairwise error probability (CPEP) of the system can be expressed as

$$P(\mathbf{X} \rightarrow \hat{\mathbf{X}} | \mathbf{g}) = Q \left(\sqrt{\frac{\delta E_s}{2N_0}} \right) \quad (11)$$

where $\delta = \|(\mathbf{X} - \hat{\mathbf{X}}) \mathbf{g}\|^2 = \mathbf{g}^H \mathbf{A} \mathbf{g}$ with $\mathbf{A} = (\mathbf{X} - \hat{\mathbf{X}})^H (\mathbf{X} - \hat{\mathbf{X}})$. By applying the alternative integral form

of the Q -function, i.e., $Q(x) = \frac{1}{\pi} \int_0^{\frac{\pi}{2}} \exp\left(-\frac{x^2}{2\sin^2\theta}\right) d\theta$, the CPEP in (11) can be rewritten as

$$P(\mathbf{X} \rightarrow \hat{\mathbf{X}}|\mathbf{g}) = \frac{1}{\pi} \int_0^{\frac{\pi}{2}} \exp\left(-\frac{\delta E_s}{4N_0 \sin^2\theta}\right) d\theta. \quad (12)$$

By integrating over the randomness of the channel coefficients, the unconditional pairwise error probability (UPEP) can be expressed as [31]

$$\begin{aligned} P(\mathbf{X} \rightarrow \hat{\mathbf{X}}) &= \frac{1}{\pi} \int_0^{\frac{\pi}{2}} E_\delta \left\{ \exp\left(-\frac{\delta E_s}{4N_0 \sin^2\theta}\right) \right\} d\theta \\ &= \frac{1}{\pi} \int_0^{\frac{\pi}{2}} \Phi_\delta\left(-\frac{E_s}{4N_0 \sin^2\theta}\right) d\theta \end{aligned} \quad (13)$$

where $\Phi_\delta(t) = E_\delta\{e^{t\delta}\}$ is the moment-generating function (MGF) of the random variable δ . For a given pair of $(\mathbf{X}, \hat{\mathbf{X}})$, using the knowledge that \mathbf{g} is a complex Gaussian vector with the mean vector $\bar{\mathbf{g}}$ and the covariance matrix \mathbf{Q} given in (9) and (10), the MGF can be obtained as [31], [32]

$$\Phi_\delta(t) = \frac{\exp\left(t\bar{\mathbf{g}}^H \mathbf{A} (\mathbf{I}_{nN_r N_t} - t\mathbf{Q}\mathbf{A})^{-1} \bar{\mathbf{g}}\right)}{\det(\mathbf{I}_{nN_r N_t} - t\mathbf{Q}\mathbf{A})}. \quad (14)$$

Using (14), the UPEP in (13) can be expressed as

$$\begin{aligned} P(\mathbf{X} \rightarrow \hat{\mathbf{X}}) &= \frac{1}{\pi} \\ &\times \int_0^{\frac{\pi}{2}} \frac{\exp\left(-\frac{E_s}{4N_0 \sin^2\theta} \bar{\mathbf{g}}^H \mathbf{A} \left(\mathbf{I}_{nN_r N_t} + \frac{E_s}{4N_0 \sin^2\theta} \mathbf{Q}\mathbf{A}\right)^{-1} \bar{\mathbf{g}}\right)}{\det\left(\mathbf{I}_{nN_r N_t} + \frac{E_s}{4N_0 \sin^2\theta} \mathbf{Q}\mathbf{A}\right)} d\theta. \end{aligned} \quad (15)$$

B. QSF-IM With Correlated Rayleigh Fading Channels

Let us consider the case of Rayleigh fading channels, i.e., $K = 0$ and $\bar{\mathbf{g}} = \mathbf{0}_{nN_r N_t \times 1}$. It follows that the MGF in (14) reduces to

$$\Phi_\delta(t) = [\det(\mathbf{I}_{nN_r N_t} - t\mathbf{Q}\mathbf{A})]^{-1} = \prod_{i=1}^v (1 - t\lambda_i)^{-1} \quad (16)$$

where λ_i are the eigen values of $\mathbf{Q}\mathbf{A}$ and $v = \text{rank}(\mathbf{Q}\mathbf{A})$. Consequently, the UPEP in (15) can be expressed as

$$\begin{aligned} P(\mathbf{X} \rightarrow \hat{\mathbf{X}}) &= \frac{1}{\pi} \int_0^{\frac{\pi}{2}} \prod_{i=1}^v \left(1 + \frac{E_s}{4N_0 \sin^2\theta} \lambda_i\right)^{-1} d\theta \\ &\leq \frac{1}{2} \prod_{i=1}^v \left(1 + \frac{E_s}{4N_0} \lambda_i\right)^{-1} \end{aligned} \quad (17)$$

where the upper bound (17) is obtained using the inequality $\sin^2\theta \leq 1$. For high signal-to-noise ratio (SNR) values, (17) can be approximated as

$$P(\mathbf{X} \rightarrow \hat{\mathbf{X}}) \leq \frac{1}{2} \left(\frac{E_s}{4N_0}\right)^{-v} \prod_{i=1}^v \frac{1}{\lambda_i}. \quad (18)$$

In addition to the integral form in (17), a closed-form expression of the UPEP can be derived by applying a closed-form approximation of the Q -function, given by [19]

$$Q(x) \approx \frac{1}{12} e^{-\frac{x^2}{2}} + \frac{1}{4} e^{-\frac{x^2}{3}}. \quad (19)$$

Substituting (19) into (11) and following the analysis in [19], it can be shown that the UPEP can be written as

$$\begin{aligned} P(\mathbf{X} \rightarrow \hat{\mathbf{X}}) &\approx \frac{1}{12} \left[\det\left(\mathbf{I}_{nN_r N_t} + \frac{E_s}{4N_0} \mathbf{Q}\mathbf{A}\right) \right]^{-1} \\ &\quad + \frac{1}{4} \left[\det\left(\mathbf{I}_{nN_r N_t} + \frac{E_s}{3N_0} \mathbf{Q}\mathbf{A}\right) \right]^{-1} \\ &= \frac{1}{12} \prod_{i=1}^v \left(1 + \frac{E_s}{4N_0} \lambda_i\right)^{-1} + \frac{1}{4} \prod_{i=1}^v \left(1 + \frac{E_s}{3N_0} \lambda_i\right)^{-1}. \end{aligned} \quad (20)$$

For high SNR values, (20) can be approximated as

$$P(\mathbf{X} \rightarrow \hat{\mathbf{X}}) \approx \left(\frac{4^v}{12} + \frac{3^v}{4}\right) \left(\frac{E_s}{N_0}\right)^{-v} \prod_{i=1}^v \frac{1}{\lambda_i}. \quad (21)$$

It can be readily seen from (18) and (21) that the diversity order and the coding gain of the system are determined by v and $\prod_{i=1}^v \lambda_i$, i.e., the rank and the eigenvalues of $\mathbf{Q}\mathbf{A}$, respectively. For the diversity order, it follows from the rank inequality [33] that $v \leq \min(\text{rank}(\mathbf{Q}), \text{rank}(\mathbf{A}))$. It is seen from (10) that \mathbf{Q} largely depends on the characteristics of the channels, i.e., power delay profiles and spatial correlation. Considering that \mathbf{Q} is full rank, it can be shown that $v \leq \min(nN_r N_t, \text{rank}(\mathbf{A})) = \text{rank}(\mathbf{A}) \leq nN_r$. It can be seen that the diversity order increases with N_r . For the coding gain, it follows that $\det(\mathbf{Q}\mathbf{A}) = \det(\mathbf{Q}) \det(\mathbf{A})$. To achieve diversity and coding benefits, *general criteria and guidelines on the design of QSF-IM schemes* can be formalized as follows:

- 1) Diversity gain: the minimum symbol-wise Hamming distance over all pairs of codewords, i.e., the minimum of $\text{rank}(\mathbf{A}) = \text{rank}\left(\left(\mathbf{X} - \hat{\mathbf{X}}\right)^H \left(\mathbf{X} - \hat{\mathbf{X}}\right)\right)$ for all $(\mathbf{X}, \hat{\mathbf{X}})$, should be maximized.
- 2) Coding gain: the minimum of $\det(\mathbf{A})$ over all codeword pairs should be maximized.

IV. ERGODIC ACHIEVABLE RATE ANALYSIS

The achievable rate of the proposed scheme is analyzed in this section. Using (3) and following the analysis in [34], the ergodic achievable sum rate of the QSF-IM scheme can be given by $R = E\{I(\mathbf{x}, \mathbf{G}; \mathbf{y})\} = E\{I(\mathbf{s}, J; \mathbf{y})\} = R_1 + R_2$ with

$$R_1 \triangleq E\{I(\mathbf{s}; \mathbf{y}|J)\} \quad (22)$$

$$R_2 \triangleq E\{I(J; \mathbf{y})\} \quad (23)$$

where the mutual information is evaluated for a given channel realization, and the expectation is averaged over all channel realizations.

A. Calculation of (22)

Conditioned a channel realization, $I(\mathbf{s}; \mathbf{y}|J)$ can be regarded as the mutual information, i.e., the achievable rate, of a deterministic MIMO channel. As a result, the sum rate analysis of MIMO channels available in the literature can be applied to compute (22). Following the analysis in Section III,

any arbitrary RB can be considered for performance evaluation. Thus, in the following discussion, the equivalent system description (3) is considered with the subscripts b being omitted for simplicity. Using (1) and (4), the transmit vector can be rewritten as $\mathbf{x} = \Upsilon_{J_I} \mathbf{x}_I + j \Upsilon_{J_Q} \mathbf{x}_Q$, with Υ_{J_I} (and Υ_{J_Q}) denoting the diagonal matrices wherein the diagonal entries corresponding to the active SF indexes J_I (and J_Q) are set to 1, and equal to 0 otherwise. Since \mathbf{x}_I and \mathbf{x}_Q are independent, equivalent as $\mathbf{x} = \Upsilon_J \mathbf{s}$ with $\Upsilon_J = \sqrt{\Upsilon_{J_I}^2 + \Upsilon_{J_Q}^2}$. Consequently, (3) can be rewritten as

$$\mathbf{y} = \sqrt{E_s} \mathbf{G} \Upsilon_J \mathbf{s} + \mathbf{w}. \quad (24)$$

The achievable rate can be given by

$$\begin{aligned} & \mathbb{E}_{\mathbf{G}} \{I(\mathbf{s}; \mathbf{y}|J)\} \\ &= \mathbb{E}_{\mathbf{G}} \left\{ \mathbb{E}_J \left\{ \log_2 \det \left(\mathbf{I}_{n_{N_r}} + \rho \mathbf{G} \Upsilon_J \Upsilon_J^H \mathbf{G}^H \right) \right\} \right\} \\ &= \mathbb{E}_{\mathbf{G}} \left\{ \mathbb{E}_J \left[\sum_{c=1}^n \log_2 \det \left(\mathbf{I}_{N_r} + \rho \mathbf{G}(c) \Upsilon_J(c) \Upsilon_J(c)^H \mathbf{G}(c)^H \right) \right] \right\} \\ &= \frac{1}{M_J} \sum_{J=1}^{M_J} \sum_{c=1}^n R_{J,c} \end{aligned} \quad (25)$$

with $R_{J,c} = \mathbb{E}_{\mathbf{G}(c)} \{ \log_2 \det \left(\mathbf{I}_{N_r} + \rho \mathbf{G}(c) \mathbf{B}_J(c) \mathbf{G}(c)^H \right) \}$ and $\rho = \frac{E_s}{N_0}$. Note that (25) is obtained from the knowledge that \mathbf{G} is a block-diagonal matrix, expressed as $\mathbf{G} = \text{blkdiag}(\mathbf{G}(1), \dots, \mathbf{G}(n))$, and Υ_J can be written as $\Upsilon_J = \text{blkdiag}(\Upsilon_J(1), \dots, \Upsilon_J(n))$. Further, (25) follows since Υ_J , for $J = 1, 2, \dots, M_J$, is equally probable, with $\mathbf{B}_J(c) = \Upsilon_J(c) \Upsilon_J(c)^H$. Notice that the term $\mathbf{G}(c) \mathbf{B}_J(c) \mathbf{G}(c)^H$ in (25) is a quadratic form of a complex Gaussian matrix $\mathbf{G}(c)$ associated with a constant Hermitian matrix $\mathbf{B}_J(c)$, and the evaluation of $R_{J,c}$ in (25) has been studied in the literature. Relevant results for correlated Rician and Rayleigh fading channels are given as follows:

1) *Correlated Rician Fading Channels*: Let $r_{J,c} = \text{rank}\{\Upsilon_J(c)\}$, and $\{\beta_{J,c}\}$ represent the set of $r_{J,c}$ active SF indexes associated to J and the subcarrier c . Denoting $\mathbf{y} = [\mathbf{y}(1)^T, \dots, \mathbf{y}(n)^T]^T$ and $\mathbf{w} = [\mathbf{w}(1)^T, \dots, \mathbf{w}(n)^T]^T$, a full-rank equivalent representation of (24) for the subcarrier c can be expressed as

$$\mathbf{y}(c) = \sqrt{E_s} \mathbf{Z}_{J,c} \mathbf{s}_{J,c} + \mathbf{w}(c) \quad (26)$$

where $\mathbf{s}_{J,c} = (\mathbf{s})^{\beta_{J,c}}$ and $\mathbf{Z}_{J,c} = \mathbf{G}_{J,c} \Upsilon_{J,c}$, with $\mathbf{G}_{J,c} = (\mathbf{G})_{\beta_{J,c}}$, $\Upsilon_{J,c} = (\Upsilon_J)_{\beta_{J,c}}$. Following the discussion in Section III-A, it can be shown that $\mathbf{Z}_{J,c}$ has a matrix-variate complex Gaussian distribution with mean matrix $\bar{\mathbf{Z}}_{J,c}$ and covariance matrix $\mathbf{Q}_{J,c}$ given by

$$\bar{\mathbf{Z}}_{J,c} = \sqrt{\frac{K}{K+1}} \left(\left[\mathbf{I}_n \otimes \bar{\mathbf{H}}(0) \right] \Upsilon_J \right)_{\beta_{J,c}} \quad (27)$$

$$\begin{aligned} \mathbf{Q}_{J,c} &= \mathbb{E} \left\{ (\mathbf{z}_{J,c} - \bar{\mathbf{z}}_{J,c})(\mathbf{z}_{J,c} - \bar{\mathbf{z}}_{J,c})^H \right\} \\ &= \frac{1}{K+1} (\mathbf{R}_r \otimes \mathbf{\Xi}_{J,c}) \end{aligned} \quad (28)$$

with $\mathbf{z}_{J,c} = \text{vec}(\mathbf{Z}_{J,c}^T)$, $\bar{\mathbf{z}}_{J,c} = \text{vec}(\bar{\mathbf{Z}}_{J,c}^T)$, and $\mathbf{\Xi}_{J,c} = (\mathbf{R}_t \Upsilon_J)_{\beta_{J,c}}$. It is seen that the achievable rate of the system

in (26) has been well investigated in the literature, e.g., the upper bounds and lower bounds given in [30] and [35] can be used as an approximation of the achievable rate. To illustrate this, the upper bound derived in [35] is applied here as an estimate of $R_{J,c}$ in (25), as written by

$$\begin{aligned} R_{J,c} &\approx \log_2 \left(\sum_{l=1}^v \left(\frac{b\rho}{N_t} \right)^l \sum_{\{a_{l,v}\}} \det(\Lambda_{a_{l,v}}^{a_{l,v}}) \sum_{\{a_{l,u}\}} \det(\Sigma_{a_{l,u}}^{a_{l,u}}) \right. \\ &\quad \left. \times (l - L_{a_{l,u}} + j + \tilde{\theta}_i^j) \tilde{\theta}_i^{j-1} \right) \quad (29) \\ &\quad \frac{\det \left((l - L_{a_{l,u}} + j + \tilde{\theta}_i^j) \tilde{\theta}_i^{j-1} \right)}{\prod_{i < j}^{L_{a_{l,u}}} (\tilde{\theta}_j - \tilde{\theta}_i)} \end{aligned}$$

where $\tilde{\theta}_1, \dots, \tilde{\theta}_{L_{a_{l,u}}}$ are the non-zero eigenvalues of

$$\tilde{\Theta}^{(a_{l,u}, a_{l,v})} = \frac{a}{b} (\Sigma_{a_{l,u}}^{a_{l,u}})^{-1} (\bar{\mathbf{M}}_{a_{l,u}}^{a_{l,u}})^H (\Lambda_{a_{l,v}}^{a_{l,v}})^{-1} (\bar{\mathbf{M}}_{a_{l,v}}^{a_{l,v}}) \quad (30)$$

with $a = \frac{K}{K+1}$, $b = \frac{1}{K+1}$, $u = \max(N_r, r_{J,c})$, $v = \min(N_r, r_{J,c})$, and

$$\Lambda = \begin{cases} \mathbf{R}_r, & N_r \leq r_{J,c} \\ \mathbf{\Xi}_{J,c}, & N_r > r_{J,c} \end{cases} \quad (31)$$

$$\Sigma = \begin{cases} \mathbf{\Xi}_{J,c}, & N_r \leq r_{J,c} \\ \mathbf{R}_r, & N_r > r_{J,c} \end{cases} \quad (32)$$

$$\bar{\mathbf{M}} = \begin{cases} \bar{\mathbf{Z}}_{J,c}, & N_r \leq r_{J,c} \\ \bar{\mathbf{Z}}_{J,c}^H, & N_r > r_{J,c}. \end{cases} \quad (33)$$

2) *Correlated Rayleigh Fading Channels*: It can be seen from (33) that, for Rayleigh fading channels with $K = 0$, $\bar{\mathbf{M}} = \mathbf{0}_{N_r \times r_{J,c}}$. Consequently, (29) can be reduced to

$$R_{J,c} \approx \log_2 \left(\sum_{l=1}^v \left(\frac{b\rho}{N_t} \right)^l l! \sum_{\{a_{l,v}\}} \det(\Lambda_{a_{l,v}}^{a_{l,v}}) \sum_{\{a_{l,u}\}} \det(\Sigma_{a_{l,u}}^{a_{l,u}}) \right). \quad (34)$$

It follows that the achievable rate R_1 in (22) can be obtained by substituting (29) (for Rician case) or (34) (for Rayleigh case) into (25).

B. Calculation of (23)

Using the property that the mutual information cannot increase by performing additional processing [36], it follows that $\mathbb{E}\{I(J; \mathbf{y})\} \geq \mathbb{E}\{I(J; \hat{\mathbf{s}}, \hat{J})\}$, with

$$\begin{aligned} I(J; \hat{\mathbf{s}}, \hat{J}) &= I(J; \hat{\mathbf{s}}|\hat{J}) + I(J; \hat{J}) \\ &= I(J; \hat{J}) = H(J) - H(J|\hat{J}) \\ &= \log_2 M_J - \frac{1}{M_J} \sum_{j=1}^{M_J} \sum_{\hat{j}=1}^{M_J} P(\hat{J} = \hat{j}|J = j) \\ &\quad \times \log_2 \frac{\sum_{j_2=1}^{M_J} P(\hat{J} = \hat{j}|J = j_2)}{P(\hat{J} = \hat{j}|J = j)} \end{aligned} \quad (35)$$

where (35) holds from the knowledge that, given that the spatial information \hat{J} is decoded, no information about J can be further obtained from $\hat{\mathbf{s}}$, i.e., $I(J; \hat{\mathbf{s}}|\hat{J}) = 0$, and (36)

follows from (35) as J is equally probable. Consequently, (23) can be expressed as

$$R_2 \geq \log_2 M_J - \mathbb{E}_G \left\{ \frac{1}{M_J} \sum_{j=1}^{M_J} \sum_{\hat{j}=1}^{M_J} P(\hat{J} = \hat{j} | J = j) \times \log_2 \frac{\sum_{j_2=1}^{M_J} P(\hat{J} = \hat{j} | J = j_2)}{P(\hat{J} = \hat{j} | J = j)} \right\} \quad (37)$$

$$\geq \log_2 M_J - \frac{1}{M_J} \sum_{j=1}^{M_J} \sum_{\hat{j}=1}^{M_J} \mathbb{E}_G \left\{ P(\hat{J} = \hat{j} | J = j) \right\} \times \log_2 \frac{\sum_{j_2=1}^{M_J} \mathbb{E}_G \left\{ P(\hat{J} = \hat{j} | J = j_2) \right\}}{\mathbb{E}_G \left\{ P(\hat{J} = \hat{j} | J = j) \right\}} \quad (38)$$

$$\approx \log_2 M_J - \frac{1}{M_J} \sum_{j=1}^{M_J} \sum_{\hat{j}=1}^{M_J} PEP(j \rightarrow \hat{j}) \times \log_2 \frac{\sum_{j_2=1}^{M_J} PEP(j_2 \rightarrow \hat{j})}{PEP(j \rightarrow \hat{j})} \quad (39)$$

where (38) is derived from (37) using the log sum inequality [36, Th. 2.7.1], and (39) follows with $\mathbb{E}_G \left\{ P(\hat{J} = \hat{j} | J = j) \right\}$ being approximated by using normalized PEPs, $PEP(j \rightarrow \hat{j})$, given as follows. First, the PEP of the transmitted spatial-modulated symbol j is decoded as \hat{j} , for $\hat{j} \neq j$, can be computed as

$$P(j \rightarrow \hat{j}) = \int_{\mathbf{s}} P(\mathbf{X} \rightarrow \hat{\mathbf{X}}) f(\mathbf{s}) ds \\ = \int_{\mathbf{s}} P((\mathbf{s}, J = j) \rightarrow (\mathbf{s}, \hat{J} = \hat{j})) f(\mathbf{s}) ds \quad (40)$$

with $f(\mathbf{s}) = \pi^{-k} \exp(-\|\mathbf{s}\|^2)$. It follows that the normalized PEPs can be defined as

$$PEP(j \rightarrow \hat{j}) = \begin{cases} \varrho_j P(j \rightarrow \hat{j}), & \text{for } \hat{j} \neq j, \\ \varrho_j \min\left(1, \sum_{\hat{j} \neq j} P(j \rightarrow \hat{j})\right), & \text{for } \hat{j} = j \end{cases} \quad (41)$$

where ϱ_j is a normalization factor such that $\sum_{\hat{j}} PEP(j \rightarrow \hat{j}) = 1$ for all j . As $PEP(j \rightarrow \hat{j})$ is used as an estimate of $\mathbb{E}_G \left\{ P(\hat{J} = \hat{j} | J = j) \right\}$, the normalization is imposed to mimic the fact that $\mathbb{E}_G \left\{ \sum_{\hat{j}} P(\hat{J} = \hat{j} | J = j) \right\} = 1$. It should, however, be noted that $PEP(j \rightarrow \hat{j})$ generally differs from $\mathbb{E}_G \left\{ P(\hat{J} = \hat{j} | J = j) \right\}$ as the former is evaluated assuming that j and \hat{j} are the only two possible codewords while all the possible codewords of j and \hat{j} are considered in the latter. By using the PEP results in Section III and substituting them into (40), (41) and (39), the achievable rate R_2 in (23) can be evaluated.

V. SPECTRAL, ENERGY, COST AND ECONOMIC EFFICIENCY TRADE-OFF

Modern wireless communication systems tend to consume more energy in order to achieve higher SE, i.e., increased data

rate, to support the growing demand for wireless data traffic. This, however, may be detrimental to the EE of the system. In general, there exists a fundamental trade-off between SE and EE, as widely studied in the literature, e.g., in [37]–[39]. In this section, trade-off between SE and EE of the proposed QSF-IM scheme will be examined. CE and ECE will also be introduced as alternative metrics for performance evaluation.

A. Spectral and Energy Efficiency

SE can be defined as the average achievable rate, in bits/s/Hz, as expressed by

$$\gamma = \frac{1}{n} \left(\frac{N}{N + N_{cp}} \right) R \quad (42)$$

where the factor $\frac{1}{n}$ reflects that R derived in Section IV is computed per RB, and $\left(\frac{N}{N + N_{cp}} \right)$ corresponds to the percentage of time for useful data transmission.

EE (in bits/Joule) is defined as a ratio of the system throughput (in bits/s) to the total power consumption (in Joule/s), as can be expressed as

$$\varepsilon = \frac{B_w \gamma}{P_c} \quad (43)$$

where B_w denotes the system bandwidth in Hz and P_c is the total power consumption, given by

$$P_c = \frac{P_{tx}}{\eta} + P_{cir} + P_0 \quad (44)$$

with P_{tx} , P_{cir} and P_0 denoting the power consumption due to signal transmission (radiated power), signal processing (RF circuit power), and other causes (static power), and η being the efficiency of the power amplifier. The radiated power is given by $P_{tx} = \left(\frac{N + N_{cp}}{N} \right) \left(\frac{k E_s}{n T_s} \right)$, with T_s being the OFDM sampling period (in seconds). The circuit power consumption can be modeled as

$$P_{cir} = P_{cod} + P_{dec} + N_t P_{RF}^{tx} + N_r (P_{RF}^{rx} + P_{SD}) \quad (45)$$

where P_{cod} , P_{dec} , P_{RF}^{tx} , P_{RF}^{rx} , and P_{SD} represent the power consumption due to channel coding, channel decoding, transmit RF chain processing, receive RF chain processing, and signal detection, respectively. Motivated by the knowledge that the number of operations of ML detection increases exponentially with data rate [7], [13], P_{SD} is modeled as $P_{SD} = \frac{2^Z}{Z T_s}$ with Z denoting the computational efficiency (in operations per Joule).

B. Cost and Economic Efficiency

In addition to SE and EE, there has been increasing interest in CE and ECE, driven by network operators' perspective, as these metrics reflect the the efficiency of the network investment and the net profitability, respectively. Various performance indicators have been proposed in the literature to evaluate the CE, such as the total network cost [40], the deployment efficiency [41], and the CE [2]. Despite being slightly difference in definitions and terminologies, these metrics have a common goal, i.e. to represent the effectiveness of

the operators' investment. In this paper, the definition of CE (in bits/monetary unit) presented in [2] will be adopted, which can be expressed as

$$\varphi = \frac{B_w \gamma}{C_{\text{tot}}} \quad (46)$$

where C_{tot} is the total cost (in monetary unit per second) modeled as

$$C_{\text{tot}} = \kappa_c P_c + C_0 \quad (47)$$

where κ_c is the energy cost per Joule (Watt-second) and C_0 involves other costs (in monetary unit per second) in addition to the energy cost, such as capital and operational expenditure. From (46), the CE indicates the number of transferable bits per unit cost. Thus, maximizing the CE would lead to the maximum revenue per unit cost, implying a sensible profit for network operators. It can be noticed, however, that the actual revenue and the net profit have not been included in the definition of the CE. To evaluate the network profitability, a novel performance indicator, referred to as ECE, has been recently studied in the literature [39], [42]. Following [39], the ECE is defined (in monetary unit per second) as

$$\varkappa = \kappa_r r_{\text{ref}} \log_2 \left(1 + \frac{B_w \gamma}{r_{\text{ref}}} \right) - C_{\text{tot}} \quad (48)$$

where κ_r is the revenue per bit and r_{ref} is a reference data rate for revenue evaluation. Note that the attainable revenue in (48) is assumed to grow logarithmically with the achievable data rate (in multiple numbers of the reference data rate), following the observation in [39] and [42].

C. SE, EE, CE and ECE Trade-Off

It can be shown that EE can be improved with increased SE when the system operates in the low SNR (low energy-consumption) regime, as demonstrated in Section VI-C. This results from the fact that a marginal increase in radiated power could significantly improve the achievable rate in this operating condition. Similarly, CE and ECE are also shown to increase with SE in this regime. However, the improvement of the achievable rate is less relevant and becomes dominated by dramatic increase in power consumption at high SNR, resulting in detrimental effect on EE, CE and ECE. Consequently, there exist optimal operating conditions that provide a balanced trade-off between SE and EE (or CE, ECE). In general, the optimum point for SE-EE trade-off may not co-locate with the optimum points for -SE-CE (or SE-ECE) trade-off, indicating that EE and CE (or ECE) cannot be maximized simultaneously. This suggests that a trade-off between EE and CE (or ECE) is generally required, i.e., an improvement of EE can only be achieved by trading it off with CE benefits and vice versa. Nevertheless, compared with existing transmission schemes, the proposed QSF-IM scheme is shown to be superior and provide better trade-offs, e.g., with respect to SE-EE, SE-CE (or SE-ECE), and EE-CE (or EE-ECE), as further elaborated in Section VI-C.

TABLE I
BASIC SIMULATION PARAMETERS

Parameters	Value
OFDM subcarrier spacing	15 kHz
Number of subcarriers (N)	128
Bandwidth (B_w)	1.92 MHz
Sampling period (T_s)	0.52 μ s
Cyclic Prefix Length (N_{cp})	16
Number of multipaths (L)	10
Power delay profile	uniform

TABLE II
POWER CONSUMPTION AND COST PARAMETERS

Parameters	Value	Parameters	Value
P_0	4 W	C_0	3.42×10^{-4} pence/s
P_{cod}	4 W	κ_c	6.33×10^{-6} pence/Joule
P_{dec}	0.5 W	κ_r	1.56×10^{-8} pence/bit
$P_{\text{RF}}^{\text{tx}}$	1 W	r_{ref}	10 Kbps
$P_{\text{RF}}^{\text{rx}}$	0.3 W	N_0	10^{-20} Watt/Hz
η	0.3	Z	10^9 operations/Joule

VI. SIMULATION RESULTS

The effectiveness of the proposed QSF-IM is evaluated numerically in this section. The basic simulation parameters are summarized in Table I. The spatial correlation is modeled using the Kronecker-based model. In particular, the correlation between the u -th and the v -th antennas is given by $[\mathbf{R}_x]_{u,v} = J_0(2\pi d_x |u - v|)$, where $x \in \{t, r\}$ represents either the transmit or the receive antenna arrays with the antenna spacing d_x (in wavelengths), and $J_0(\cdot)$ denotes the zero-th order Bessel function of the first kind. In this paper, it is assumed that $d_t = d_r = d$. The SNR is defined as $\left(\frac{N+N_{\text{cp}}}{N}\right) \left(\frac{k}{n}\right) \frac{E_s}{N_0}$ and $E_b/N_0 = \left(\frac{N+N_{\text{cp}}}{N}\right) \left(\frac{k}{m}\right) \frac{E_s}{N_0}$. Moreover, motivated by [41] and [43]–[45], the power consumption and cost parameters are given in Table II. For practical evaluation of the radiated power P_{tx} , the distance between the transmitter and the receiver is also assumed to be 1000 meters with pathloss exponent being 3.8.

A. BER Performance

The BER performance over correlated Rayleigh fading channels is evaluated in Figs. 2 and 3. Here, the configuration $(N_r, N_t, n, k, M) = (2, 2, 4, 1, 4)$ is assumed, corresponding to $m = 8$ bits/RB. As can be seen from Fig. 2, an increase in spatial correlation results in degradation in BER performance as the spatial signature becomes less distinguishable with higher spatial correlation. This property is inherited from the SM scheme as also discussed in [12]. Nevertheless, the BER performance can be significantly improved with the number of received antennas N_r , as illustrated in Fig. 3. Notice an improvement of diversity order (a deeper slope of the BER curves) as N_r increases, conforming with the discussion in Section III. It is also shown in Figs. 2 and 3 that the theoretical upper bounds as analyzed in Section are tight, especially

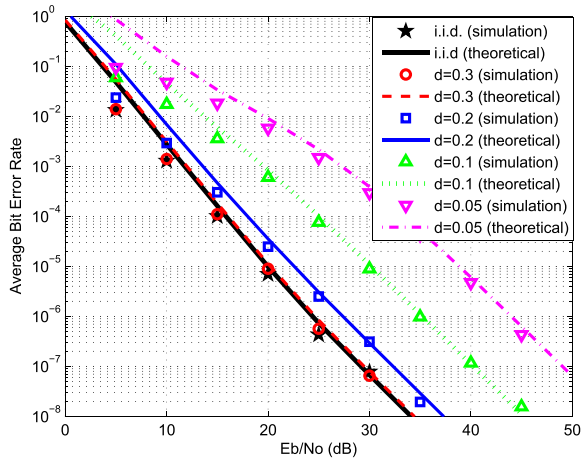


Fig. 2. BER performance of the proposed QSF-IM scheme for independent and identically distributed (i.i.d.) Rayleigh fading channels, and correlated Rayleigh fading channels with different antenna spacings d (in wavelengths) and configuration $(N_r, N_t, n, k, M) = (2, 2, 4, 1, 4)$.

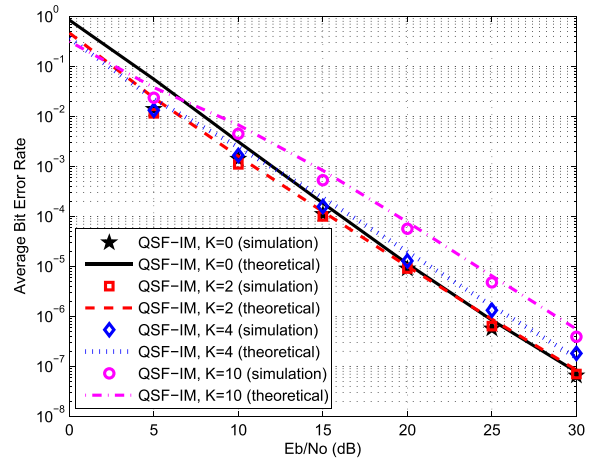


Fig. 5. BER performance of the QSF-IM scheme for Rician fading channels with different K factors, $d = 0.3$ (wavelengths), and $(N_r, N_t, n, k, M) = (2, 2, 4, 1, 4)$.

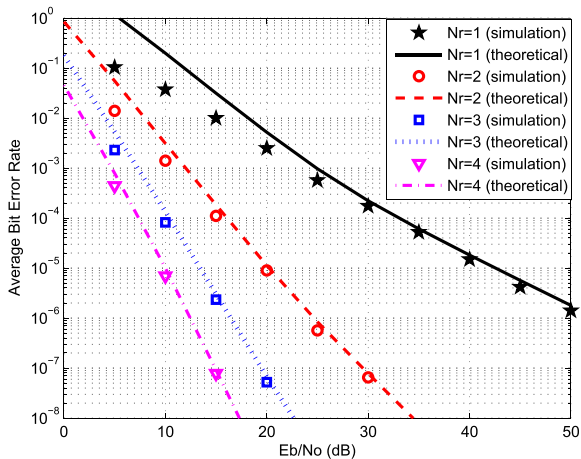


Fig. 3. BER performance of the proposed QSF-IM scheme for Rayleigh fading channels with various N_r , $d = 0.3$ (wavelengths) and $(N_r, N_t, n, k, M) = (2, 4, 1, 4)$.

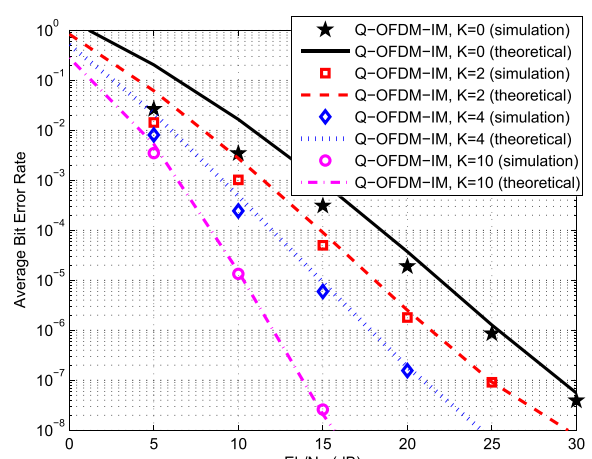


Fig. 6. BER performance of the Q-OFDM-IM scheme for Rician fading channels with different K factors, $d = 0.3$ (wavelengths), and $(N_r, N_t, n, k, M) = (2, 1, 4, 2, 4)$.

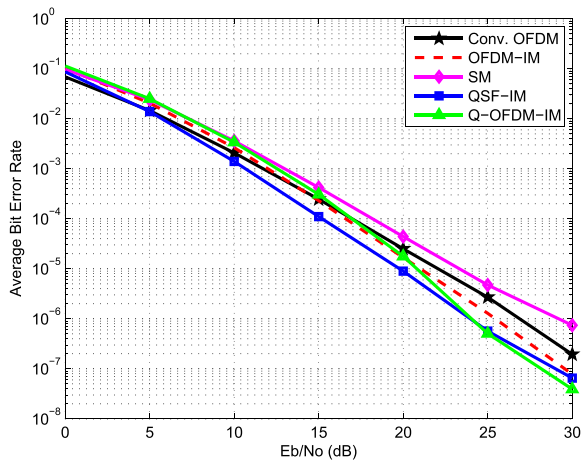


Fig. 4. Comparison of BER performance for Rayleigh fading channels with $N_r = 2$ and $d = 0.3$ (wavelengths).

at high SNR, verifying the correctness of the theoretical derivations as well as the simulations.

Fig. 4 presents a comparison of the QSF-IM scheme with existing techniques at the same data rate ($m = 8$ bits/RB),

i.e., the conventional OFDM (Conv. OFDM), the OFDM-IM, and the SM schemes with configurations $(N_r, N_t, n, k, M) = (2, 1, 4, 4, 4)$, $(2, 1, 4, 3, 4)$, and $(2, 2, 4, 4, 2)$, respectively. Note that, for the SM scheme, SM is applied to each subcarrier. It is seen that the proposed QSF-IM scheme outperforms the aforementioned techniques. The performance of Q-OFDM-IM with configuration $(N_r, N_t, n, k, M) = (2, 1, 4, 2, 4)$ is also given in Fig. 4. Comparing with QSF-IM, Q-OFDM-IM deploys a single transmit antenna, i.e., no transmit spatial correlation, leading to superior performance in the high SNR regime. Nevertheless, the QSF-IM scheme tends to be more appropriate for the practical, i.e., low-to-moderate, SNR regime.

The BER performance of the proposed QSF-IM and Q-OFDM-IM schemes over correlated Rician fading channels is presented in Figs. 5 and 6, respectively. While the line-of-sight (LOS) components lead to higher spatial correlation which, in turn, degrades BER performance, they reduce the impacts of channel fading, e.g., strengthen the channel gains

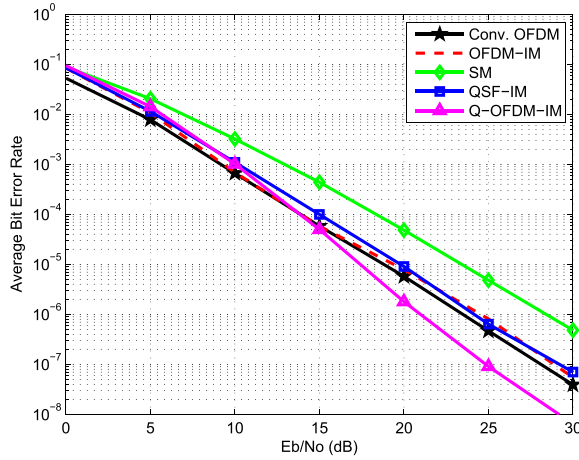


Fig. 7. Comparison of BER performance for Rician fading channels with $K = 2$, $N_r = 2$ and $d = 0.3$ (wavelengths).

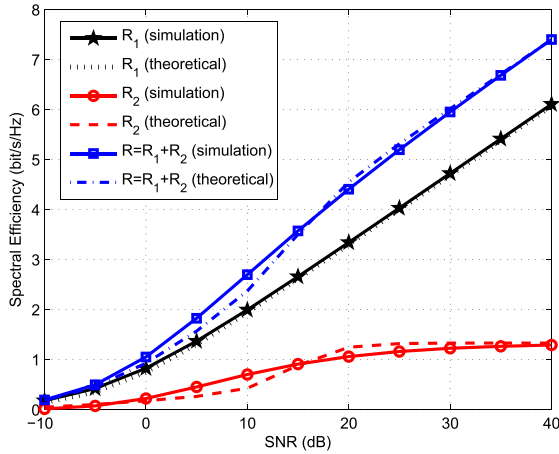


Fig. 8. Achievable sum rate of the proposed QSF-IM scheme for Rayleigh fading channels with configuration $(N_r, N_t, n, k) = (2, 2, 4, 1)$ and $d = 0.3$ (wavelengths).

of each subcarrier in the frequency domain, resulting in the improvement of BER. With the contradicting effects of LOS components being compromised for small K , no significant difference in BER performance of QSF-IM is observed for $0 \leq K \leq 2$. For higher K values, however, the impact of higher spatial correlation becomes dominant, leading to degradation on the average BER, as demonstrated in Fig. 5. In contrast, the Q-OFDM-IM scheme can avoid the detrimental effect of the transmit spatial correlation with a single transmit antenna. As a result, the BER of Q-OFDM-IM improves as K increases, as depicted in 6. Comparing the existing algorithms in Fig. 7, Q-OFDM-IM offers a good solution for deployment scenarios with strong LOS and high spatial correlation.

B. Achievable Rate

The theoretical achievable sum rate of the QSF-IM scheme with $(N_r, N_t, n, k) = (2, 2, 4, 1)$ is evaluated for Rayleigh fading channels in Fig. 8. The contribution of R_1 given in (34) is shown to match well with simulation results. The theoretical derivation in (39) is also seen to be a good estimate

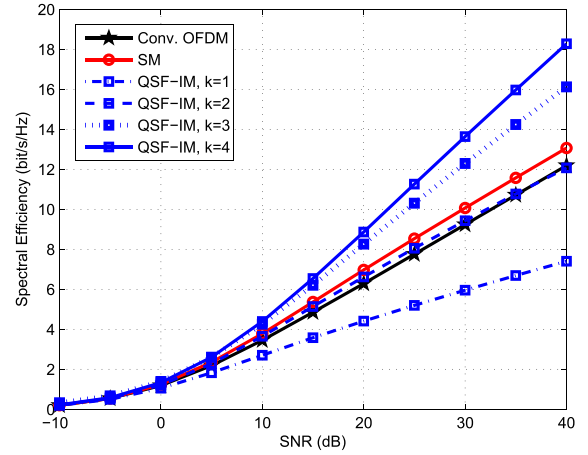


Fig. 9. Achievable sum rate of the QSF-IM scheme for Rayleigh fading channels with $d = 0.3$ (wavelengths) and different numbers of active SF indexes, k .

of R_2 , despite PEPs being used for approximation. This suggests that the theoretical analysis given in Section IV can generally be used for the achievable sum rate approximation. The achievable sum rates of the proposed QSF-IM scheme with $(N_r, N_t, n) = (2, 2, 4)$ and various numbers of active SF indexes, k , are presented in Fig. 9. For Conv. OFDM and SM, $(N_r, N_t, n, k) = (2, 1, 4, 4)$ and $(N_r, N_t, n, k) = (2, 2, 4, 4)$ are considered. By increasing k , more independent data streams are transmitted on the available SF resources for each RB, leading to the increase in spatial multiplexing gain as can be observed through the slopes of the SE curves. Notice that, by decomposing the modulated symbols into in-phase and quadrature-phase components and spatially modulating them using two independent (in-phase and quadrature-phase) spatial constellations, the effective number of active SF resources of QSF-IM scheme can be greater than k for each RB. Consequently, comparing to Conv. OFDM and SM schemes with $k = 4$, the proposed QSF-IM can achieve higher multiplexing gain with smaller or equal values of k , e.g., $k = 3, 4$, as demonstrated in Fig. 9. A similar conclusion can be drawn by comparing Q-OFDM-IM with OFDM-IM schemes, both with configuration $(N_r, N_t, n) = (2, 1, 4)$, as illustrated in Fig. 10, indicating the advantages of the proposed schemes over the existing techniques.

C. Trade-Off Between SE, EE, CE and ECE

Trade-offs between EE and SE for the proposed as well as existing schemes are presented in Fig. 11. The EE is shown to grow with the SE at low SNR due to the significant increase in achievable rate with a small increase in energy consumption in this regime. In contrast, the improvement of achievable rate becomes overwhelmed by the dramatic increase in energy consumption, resulting in the reduction of EE, at high SNR. There exist optimal points that can achieve a balanced trade-off between EE and SE, as illustrated by *point A* in Fig 11. It can also be seen that the proposed QSF-IM schemes, e.g., with $k = 3, 4$, are superior and can achieve better EE and SE, comparing with existing schemes.

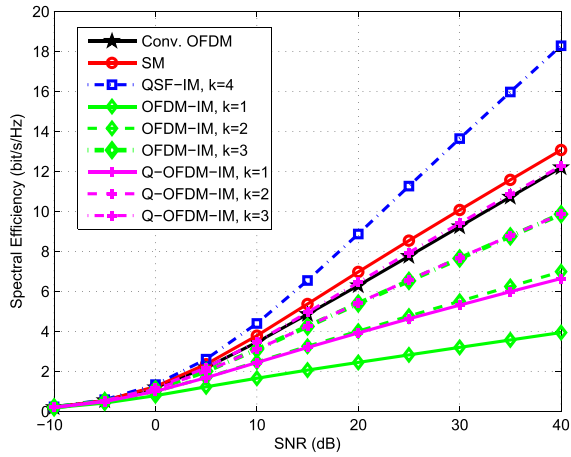


Fig. 10. Achievable sum rate of the Q-OFDM-IM scheme for Rayleigh fading channels with $d = 0.3$ (wavelengths) and different numbers of active SF indexes, k .

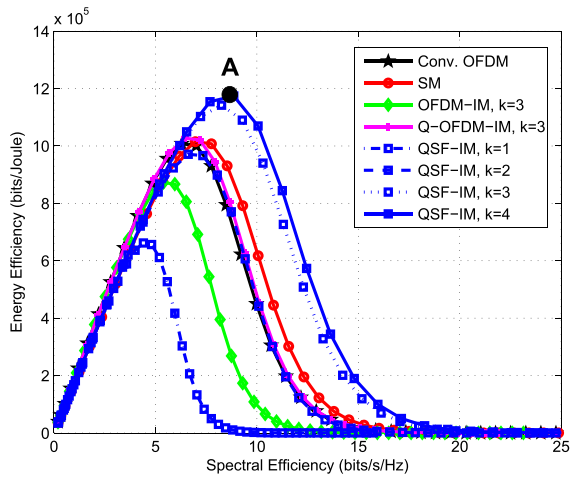


Fig. 11. EE versus SE for Rayleigh fading channels with $d = 0.3$ (wavelengths) and $N_r = 2$.

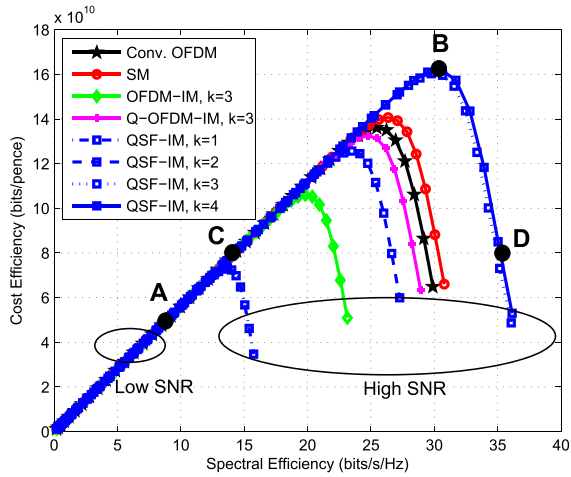


Fig. 12. CE versus SE for Rayleigh fading channels with $d = 0.3$ (wavelengths) and $N_r = 2$.

CE and ECE are also evaluated in Figs. 12 and 13, respectively. Trade-offs between CE/ECE and SE can be shown, as similarly discussed in Fig. 11. It is also seen that the optimum

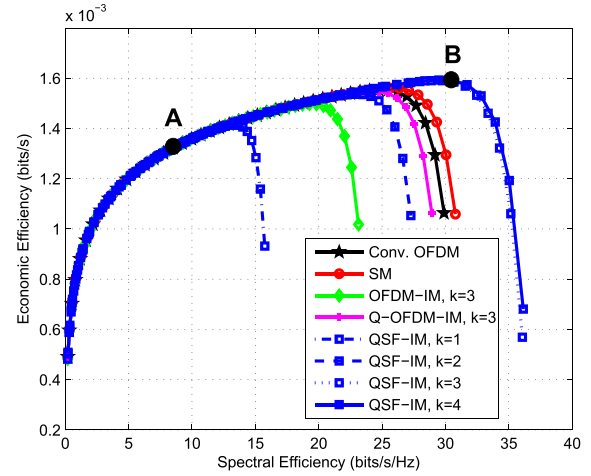


Fig. 13. ECE versus SE for Rayleigh fading channels with $d = 0.3$ (wavelengths) and $N_r = 2$.

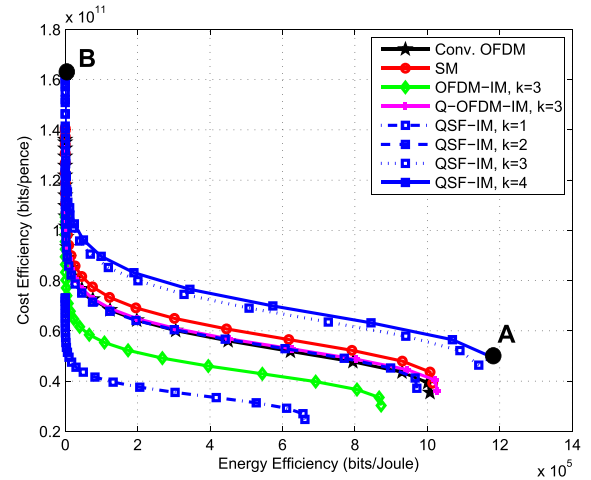


Fig. 14. Trade-off between CE and EE for Rayleigh fading channels with $d = 0.3$ (wavelengths) and $N_r = 2$.

point of CE appears to co-locate with that of ECE, denoted as *point B*, in this experiment. It should be noted, however, that the optimum points of CE and ECE may differ, in general, depending on the power consumption and cost models as well as their associated parameters. In contrast, the optimum point of EE (*point A*) does not usually coexist with that of CE and ECE (*point B*). As a result, a performance trade-off between EE and CE/ECE, i.e., between the points *A* and *B*, is generally required, as demonstrated for CE-EE trade-off in Fig. 14 (similar results can be obtained for ECE-EE trade-off and, therefore, are omitted). As can be seen in Fig. 14, an increase in CE can be attained by trading it off with EE advantages. Nevertheless, the proposed QSF-IM schemes with $k = 3, 4$ achieve the better trade-off curves, compared with other schemes.

It should also be noted that, although ECE is directly proportional to CE, the values of ECE can significantly vary with the operating points. For instance, consider two points with the same CE, i.e., *points C and D* in Fig. 12. It can be shown in Fig. 15 that the point *C*, corresponding to low SNR (low power consumption), achieves higher ECE

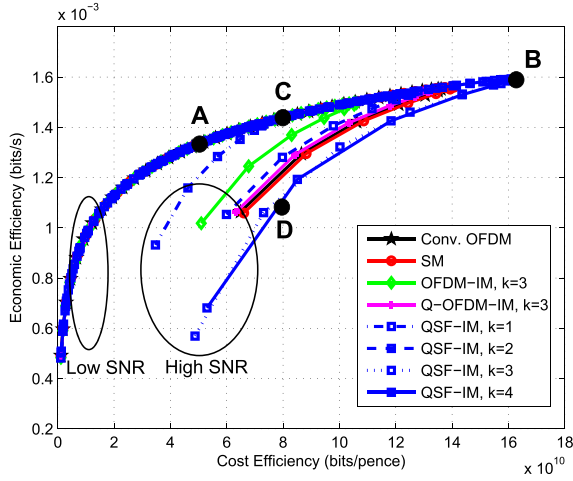


Fig. 15. ECE versus CE for Rayleigh fading channels with $d = 0.3$ (wavelengths) and $N_r = 2$.

(higher net profit) due to much lower energy cost. This suggests that, at the same CE, a network that operates at lower energy consumption, despite providing lower data rate, tends to be more economically efficient and offer more net profits than that operates at more power with higher data rate. This emphasizes the importance of green communications from the economical and network operators' perspective. Compared with other schemes, the proposed QSF-IM scheme is shown to be a promising candidate for green communications that achieves a better trade-off between SE and EE as well as between CE/CE and EE and offers higher economical benefits, as demonstrated through Figs. 11 - 15.

VII. CONCLUSIONS

In this paper, a novel QSF-IM scheme has been proposed as a potential wireless technology for energy-efficient 5G systems. The proposed scheme generalizes the idea of QSM and exploits its benefits of using dual antenna constellation across the spatial and frequency domains. The theoretical BER and the achievable sum-rate of the proposed scheme over frequency-selective correlated Rician and Rayleigh fading channels have been derived. It has been shown that strong LOS leads to adverse effects in the spatial domain due to increased spatial correlation, whereas it could strengthen the channel gains, i.e., reducing the fading effects, in the frequency domain, resulting in performance enhancement. This suggests that a design of QSF-IM constellation with a small number of antenna indexes (possibly with a relatively large number of frequency indexes) would be suitable for LOS scenarios. A comprehensive study of performance trade-offs between SE, EE, CE, and ECE has also been given. In particular, it has been shown that the maximum points of EE and CE typically do not coexist. As a result, an improvement of CE can be achieved, in general, by trading it off with EE advantages, and vice versa. Nevertheless, the proposed scheme has been shown to outperform the existing transmission schemes and achieve better performance in terms of SE-EE, SE-CE (or SE-ECE), and EE-CE (or EE-ECE) trade-offs, stressing the feasibility

and suitability of the proposed scheme as a potential energy-efficient technique for future 5G wireless systems.

VIII. FUTURE WORK

The proposed schemes in this paper can further be improved and extended in several aspects, some of which are outlined as follows.

- 1) It has been shown in Section II-C that the ML detector has exponential increasing complexity, which tends to be infeasible for practical implementation, especially with higher order modulation and higher MIMO schemes. A further study on the low-complexity detection algorithms for the proposed schemes, as similarly discussed for other IM-based schemes in [22] and [24]–[26], is therefore one of the key potential improvements of this work.
- 2) The diversity order achieved by the proposed scheme has been analyzed at the end of Section III, and is simply shown to increase with N_r . More detailed analysis on the diversity order, and its dependencies on other factors, e.g., the number of modulated symbols per RB (k), should be further investigated.
- 3) Based upon the general design guidelines given at the end of Section III, practical designs of the proposed QSF-IM schemes, e.g., the design of SF-index constellation for in-phase and quadrature-phase components, could be one of the interesting tasks for further studies.

APPENDIX A CHANNEL MODELS

A correlated frequency-selective Rician fading channels can be represented by a tapped-delay channel model, with the channel matrix corresponding to an l -th tap (multipath) given by

$$\mathbf{H}(l) = \sqrt{\frac{K}{K+1}} \sqrt{\psi_l} \bar{\mathbf{H}}(l) + \sqrt{\frac{1}{K+1}} \sqrt{\omega_l} \check{\mathbf{H}}(l) \quad (49)$$

where $\bar{\mathbf{H}}(l), \check{\mathbf{H}}(l) \in \mathbb{C}^{N_r \times N_t}$ represent the LOS and non-line-of-sight (NLOS) components of the l -th tap, and K denotes the Rician K-factor. The parameters ψ_l and ω_l indicate the power of LOS and NLOS components of the l -th multipath, with $\sum_{l=0}^{L-1} \psi_l = 1$, $\sum_{l=0}^{L-1} \omega_l = 1$, and L denoting the number of taps. Following [5] and [30], the LOS components can be modeled as

$$\bar{\mathbf{H}}(l) = \begin{cases} \mathbf{a}(\theta_r) \mathbf{a}(\theta_t)^H, & l = 0 \\ \mathbf{0}_{N_r \times N_t}, & l = 1, 2, \dots, L-1 \end{cases} \quad (50)$$

with $\mathbf{a}(\theta_r) = [1, e^{-j2\pi d_r \cos(\theta_r)}, \dots, e^{-j2\pi(N_r-1)d_r \cos(\theta_r)}]^T$ and $\mathbf{a}(\theta_t) = [1, e^{-j2\pi d_t \cos(\theta_t)}, \dots, e^{-j2\pi(N_t-1)d_t \cos(\theta_t)}]^T$, where θ_r and θ_t denote the angle of arrival (AoA) and the angle of departure (AoD), respectively. Both angles are assumed to be uniformly distributed on $[0, 2\pi]$. The variables d_r and d_t represent the antenna spacings, in wavelengths, of the receive and transmit antenna arrays, respectively. The NLOS components are assumed to be spatially correlated, i.e., the channel matrix is given by $\check{\mathbf{H}}(l) = \mathbf{R}_r^{\frac{1}{2}} \check{\mathbf{H}}_w(l) \mathbf{R}_t^{\frac{T}{2}}$, with \mathbf{R}_r

and \mathbf{R}_l denoting the receive and transmit spatial correlation matrices, and each element of $\check{\mathbf{H}}_w(l)$ being i.i.d. complex Gaussian variable with zero mean and unit variance.

Letting $\mathbf{H}_T = [\text{vec}(\mathbf{H}(0)^T), \dots, \text{vec}(\mathbf{H}(L-1)^T)]^T \in \mathbb{C}^{L \times N_r N_t}$, $\check{\mathbf{H}}_T = [\text{vec}(\check{\mathbf{H}}(0)^T), \dots, \text{vec}(\check{\mathbf{H}}(L-1)^T)]^T \in \mathbb{C}^{L \times N_r N_t}$, and $\check{\check{\mathbf{H}}}_T = [\text{vec}(\check{\check{\mathbf{H}}}(0)^T), \dots, \text{vec}(\check{\check{\mathbf{H}}}(L-1)^T)]^T \in \mathbb{C}^{L \times N_r N_t}$, the channel coefficients in the time domain can be written as

$$\mathbf{H}_T = \sqrt{\frac{K}{K+1}} \sqrt{\Psi} \check{\mathbf{H}}_T + \sqrt{\frac{1}{K+1}} \sqrt{\Omega} \check{\check{\mathbf{H}}}_T \quad (51)$$

with $\Psi = \text{diag}(\psi_0, \psi_1, \dots, \psi_{L-1}) \in \mathbb{C}^{L \times L}$ and $\Omega = \text{diag}(\omega_0, \omega_1, \dots, \omega_{L-1}) \in \mathbb{C}^{L \times L}$. Note that according to (50), ψ_l equals 1 for $l = 0$ and equals 0 otherwise. Let $\mathbf{H}_{T,p} \in \mathbb{C}^{N \times N_r N_t}$ be the zero-padded version of \mathbf{H}_T , such that zeros are added from the row $L+1$ to the row N , it can be shown that

$$\mathbf{H}_{T,p} = \sqrt{\frac{K}{K+1}} \sqrt{\Psi_p} \check{\mathbf{H}}_T + \sqrt{\frac{1}{K+1}} \sqrt{\Omega_p} \check{\check{\mathbf{H}}}_T \quad (52)$$

with $\Psi_p = [\Psi^T, \mathbf{0}_{L \times (N-L)}]^T \in \mathbb{C}^{N \times L}$ and $\Omega_p = [\Omega^T, \mathbf{0}_{L \times (N-L)}]^T \in \mathbb{C}^{N \times L}$. Considering the case that the channel is constant during the transmission of an OFDM block and the length of cyclic prefix (N_{cp}) is larger than L , the channel coefficients in the frequency domain, $\mathbf{G} \in \mathbb{C}^{N \times N_r N_t}$, can be given by

$$\mathbf{H}_F = \mathbf{W}_N \mathbf{H}_{T,p}. \quad (53)$$

By denoting $\mathbf{g}_b(c)^T \in \mathbb{C}^{1 \times N_r N_t}$ as the channel coefficients of the c -th subcarrier in the b -th RB, i.e., the C -th row of \mathbf{H}_F where $C = (b-1)n + c$, and $\mathbf{G}_b(c) = \text{ivec}(\mathbf{g}_b(c), N_t, N_r)^T \in \mathbb{C}^{N_r \times N_t}$, an equivalent channel matrix of the b -th RB in the frequency domain, $\mathbf{G}_b \in \mathbb{C}^{n N_r \times n N_t}$, can be given as

$$\mathbf{G}_b = \text{blkdiag}\{\mathbf{G}_b(c)\}_{c \in \{1, \dots, n\}}. \quad (54)$$

APPENDIX B

DERIVATION OF MEAN VECTOR AND COVARIANCE MATRIX

From (53) and (8), it can be shown that \mathbf{g}_F can be written as $\mathbf{g}_F = \text{vec}(\mathbf{H}_F^T)$. By substituting (52) into (53), it follows that $\mathbf{g}_F = \check{\mathbf{g}}_F + \check{\check{\mathbf{g}}}_F$ with

$$\check{\mathbf{g}}_F = \sqrt{\frac{K}{K+1}} \text{vec}\left([\mathbf{W}_N \sqrt{\Psi_p} \check{\mathbf{H}}_T]^T\right) \quad (55)$$

$$\check{\check{\mathbf{g}}}_F = \sqrt{\frac{1}{K+1}} \text{vec}\left([\mathbf{W}_N \sqrt{\Omega_p} \check{\check{\mathbf{H}}}_T]^T\right). \quad (56)$$

It can be seen that \mathbf{g}_F is a complex Gaussian vector with mean vector $\check{\mathbf{g}}_F$ and covariance matrix $\mathbf{Q}_F = \text{E}\{(\mathbf{g}_F - \check{\mathbf{g}}_F)(\mathbf{g}_F - \check{\mathbf{g}}_F)^H\} = \text{E}\{\check{\check{\mathbf{g}}}_F \check{\check{\mathbf{g}}}_F^H\}$. For the mean vector $\check{\mathbf{g}}_F$, using the knowledge that only the $(1, 1)$ -th element of $\check{\mathbf{g}}_F$ is non-zero, i.e., ψ_l equal to 1 for $l = 0$ and equal to 0 otherwise, it can be shown that $\sqrt{\Psi_p} \check{\mathbf{H}}_T = \mathbf{e}_1 \text{vec}(\check{\mathbf{H}}(0)^T)^T$, where \mathbf{e}_1 is a unit vector with the first entry being 1 and the

others being 0. Further, using $\mathbf{W}_N \mathbf{e}_1 = \mathbf{1}_N$ and $\text{vec}(\mathbf{AXB}) = (\mathbf{B}^T \otimes \mathbf{A}) \text{vec}(\mathbf{X})$, (55) can be rewritten as

$$\begin{aligned} \check{\mathbf{g}}_F &= \sqrt{\frac{K}{K+1}} \text{vec}\left(\text{vec}(\check{\mathbf{H}}(0)^T) \mathbf{1}_N^T\right) \\ &= \sqrt{\frac{K}{K+1}} (\mathbf{1}_N \otimes \mathbf{I}_{N_r N_t}) \text{vec}(\check{\mathbf{H}}(0)^T). \end{aligned} \quad (57)$$

For the covariance matrix \mathbf{Q}_F , using $\text{vec}\left([\mathbf{W}_N \sqrt{\Omega_p} \check{\check{\mathbf{H}}}_T]^T\right) = \text{vec}(\check{\check{\mathbf{H}}}_T^T \sqrt{\Omega_p^T} \mathbf{W}_N^T) = (\mathbf{W}_N \sqrt{\Omega_p} \otimes \mathbf{I}_{N_r N_t}) \text{vec}(\check{\check{\mathbf{H}}}_T^T)$, it can be derived from (56) that

$$\begin{aligned} \mathbf{Q}_F &= \text{E}\{\check{\check{\mathbf{g}}}_F \check{\check{\mathbf{g}}}_F^H\} \\ &= \frac{1}{K+1} (\mathbf{W}_N \sqrt{\Omega_p} \otimes \mathbf{I}_{N_r N_t}) \\ &\quad \text{E}\left\{\text{vec}(\check{\check{\mathbf{H}}}_T^T) \text{vec}(\check{\check{\mathbf{H}}}_T^T)^H\right\} (\mathbf{W}_N \sqrt{\Omega_p} \otimes \mathbf{I}_{N_r N_t})^H \end{aligned} \quad (58)$$

$$\begin{aligned} &= \frac{1}{K+1} (\mathbf{W}_N \sqrt{\Omega_p} \otimes \mathbf{I}_{N_r N_t}) \\ &\quad \times \{\mathbf{I}_L \otimes (\mathbf{R}_r \otimes \mathbf{R}_t)\} (\mathbf{W}_N \sqrt{\Omega_p} \otimes \mathbf{I}_{N_r N_t})^H \end{aligned} \quad (59)$$

$$= \frac{1}{K+1} (\mathbf{W}_N \Omega \mathbf{W}_N^H) \otimes (\mathbf{R}_r \otimes \mathbf{R}_t) \quad (60)$$

where (59) follows from (58) using the knowledge that $\check{\mathbf{H}}(l_i)$ and $\check{\mathbf{H}}(l_j)$ are statistically independent for $l_i \neq l_j$, and $\text{E}\left\{\text{vec}(\check{\mathbf{H}}(l)^T) \text{vec}(\check{\mathbf{H}}(l)^T)^H\right\} = \mathbf{R}_r \otimes \mathbf{R}_t$ for all $l = 0, \dots, L-1$.

REFERENCES

- [1] C.-X. Wang *et al.*, "Cellular architecture and key technologies for 5G wireless communication networks," *IEEE Commun. Mag.*, vol. 52, no. 2, pp. 122–130, Feb. 2014.
- [2] IMT-2020 (5G) Promotion Group, "5G vision and requirements," Beijing, China, White Paper 910, May 2014.
- [3] A. J. Paulraj, D. A. Gore, R. U. Nabar, and H. Bolcskei, "An overview of MIMO communications—A key to gigabit wireless," *Proc. IEEE*, vol. 92, no. 2, pp. 198–218, Feb. 2004.
- [4] A. J. Paulraj, R. U. Nabar, and D. A. Gore, *Introduction to Space-Time Wireless Communications*. Cambridge, U.K.: Cambridge Univ. Press, 2003.
- [5] D. Tse and P. Viswanath, *Fundamentals of Wireless Communication*. Cambridge, U.K.: Cambridge Univ. Press, 2005.
- [6] C.-X. Wang, S. Wu, L. Bai, X. You, J. Wang, and C.-L. I, "Recent advances and future challenges for massive MIMO channel measurements and models," *Sci. China Inf. Sci.*, vol. 59, no. 2, p. 021301, 2016.
- [7] R. Y. Mesleh, H. Haas, S. Sinanovic, C. W. Ahn, and S. Yun, "Spatial modulation," *IEEE Trans. Veh. Technol.*, vol. 57, no. 4, pp. 2228–2241, Jul. 2008.
- [8] M. Di Renzo, H. Haas, A. Ghayeb, S. Sugiura, and L. Hanzo, "Spatial modulation for generalized MIMO: Challenges, opportunities, and implementation," *Proc. IEEE*, vol. 102, no. 1, pp. 56–103, Jan. 2014.
- [9] M. Di Renzo, H. Haas, and P. M. Grant, "Spatial modulation for multiple-antenna wireless systems: A survey," *IEEE Commun. Mag.*, vol. 49, no. 12, pp. 182–191, Dec. 2011.
- [10] E. Basar, "Index modulation techniques for 5G wireless networks," *IEEE Commun. Mag.*, vol. 54, no. 7, pp. 168–175, Jul. 2016.
- [11] J. Jeganathan, A. Ghayeb, L. Szczecinski, and A. Ceron, "Space shift keying modulation for MIMO channels," *IEEE Trans. Wireless Commun.*, vol. 8, no. 7, pp. 3692–3703, Jul. 2009.

- [12] M. Di Renzo and H. Haas, "Space shift keying (SSK-) MIMO over correlated Rician fading channels: Performance analysis and a new method for transmit-diversity," *IEEE Trans. Commun.*, vol. 59, no. 1, pp. 116–129, Jan. 2011.
- [13] A. Younis, N. Serafimovski, R. Mesleh, and H. Haas, "Generalised spatial modulation," in *Proc. Asilomar Conf. Signals, Syst. Comput.*, Pacific Grove, CA, USA, Nov. 2010, pp. 1498–1502.
- [14] J. Wang, S. Jia, and J. Song, "Generalised spatial modulation system with multiple active transmit antennas and low complexity detection scheme," *IEEE Trans. Wireless Commun.*, vol. 11, no. 4, pp. 1605–1615, Apr. 2012.
- [15] Y. Xiao, Z. Yang, L. Dan, P. Yang, L. Yin, and W. Xiang, "Low-complexity signal detection for generalized spatial modulation," *IEEE Commun. Lett.*, vol. 18, no. 3, pp. 403–406, Mar. 2014.
- [16] A. Stavridis, S. Sinanovic, M. Di Renzo, and H. Haas, "Transmit precoding for receive spatial modulation using imperfect channel knowledge," in *Proc. IEEE VTC-Spring*, Yokohama, Japan, May 2012, pp. 1–5.
- [17] R. Zhang, L.-L. Yang, and L. Hanzo, "Generalised pre-coding aided spatial modulation," *IEEE Trans. Wireless Commun.*, vol. 12, no. 11, pp. 5434–5443, Nov. 2013.
- [18] M. I. Kadir, L. Hanzo, S. Chen, and S. Sugiura, "Unified MIMO-multicarrier designs: A space-time shift keying approach," *IEEE Commun. Surveys Tuts.*, vol. 17, no. 2, pp. 550–579, 2nd Quart., 2015.
- [19] E. Başar, U. Aygözü, E. Panayircı, and H. Poor, "Orthogonal frequency division multiplexing with index modulation," *IEEE Trans. Signal Process.*, vol. 61, no. 22, pp. 5536–5549, Nov. 2013.
- [20] T. Datta, H. S. Eshwaraiah, and A. Chockalingam, "Generalized space-and-frequency index modulation," *IEEE Trans. Veh. Technol.*, vol. 65, no. 7, pp. 4911–4924, Jul. 2016.
- [21] R. Fan, Y. J. Yu, and Y. L. Guan, "Generalization of orthogonal frequency division multiplexing with index modulation," *IEEE Trans. Wireless Commun.*, vol. 14, no. 10, pp. 5350–5359, Oct. 2015.
- [22] B. Zheng, F. Chen, M. Wen, F. Ji, H. Yu, and Y. Liu, "Low-complexity ML detector and performance analysis for OFDM With in-phase/quadrature index modulation," *IEEE Commun. Lett.*, vol. 19, no. 11, pp. 1893–1896, Nov. 2015.
- [23] Y. Xiao, S. Wang, L. Dan, X. Lei, P. Yang, and W. Xiang, "OFDM with interleaved subcarrier-index modulation," *IEEE Commun. Lett.*, vol. 18, no. 8, pp. 1447–1450, Aug. 2014.
- [24] E. Başar, "Multiple-input multiple-output OFDM with index modulation," *IEEE Signal Process. Lett.*, vol. 22, no. 12, pp. 2259–2263, Dec. 2015.
- [25] B. Zheng, M. Wen, E. Basar, and F. Chen, "Multiple-input multiple-output OFDM with index modulation: Low-complexity detector design," *IEEE Trans. Signal Process.*, vol. 65, no. 11, pp. 2758–2772, Jun. 2017.
- [26] L. Wang, Z. Chen, Z. Gong, and M. Wu, "Space-frequency coded index modulation with linear-complexity maximum likelihood receiver in the MIMO-OFDM system," *IEEE Signal Process. Lett.*, vol. 23, no. 10, pp. 1439–1443, Oct. 2016.
- [27] H.-W. Liang, R. Chang, W.-H. Chung, H. Zhang, and S.-Y. Kuo, "Bi-space shift keying modulation for MIMO systems," *IEEE Commun. Lett.*, vol. 16, no. 8, pp. 1161–1164, Aug. 2012.
- [28] R. Mesleh, S. S. Ikki, and H. M. Aggoune, "Quadrature spatial modulation," *IEEE Trans. Veh. Technol.*, vol. 64, no. 6, pp. 2738–2742, Jun. 2015.
- [29] R. Mesleh, S. S. Ikki, and H. M. Aggoune, "Quadrature spatial modulation-performance analysis and impact of imperfect channel knowledge," *Trans. Emerg. Telecommun. Technol.*, vol. 28, no. 1, 2014, doi: 10.1002/ett.2905.
- [30] M. R. McKay and I. B. Collings, "General capacity bounds for spatially correlated Rician MIMO channels," *IEEE Trans. Inf. Theory*, vol. 51, no. 9, pp. 3121–3145, Sep. 2005.
- [31] A. Hedayat, H. Shah, and A. Nosratinia, "Analysis of space-time coding in correlated fading channels," *IEEE Trans. Wireless Commun.*, vol. 4, no. 6, pp. 2882–2891, Nov. 2005.
- [32] G. L. Turin, "The Characteristic Function of Hermitian Quadratic Forms in Complex Normal Variables," *Biometrika*, vol. 47, nos. 1–2, pp. 199–201, 1960.
- [33] R. A. Horn and C. R. Johnson, *Matrix Analysis*. Cambridge, U.K.: Cambridge Univ. Press, 1985.
- [34] Y. Yang and B. Jiao, "Information-guided channel-hopping for high data rate wireless communication," *IEEE Commun. Lett.*, vol. 12, no. 4, pp. 225–227, Apr. 2008.
- [35] M. McKay, P. Smith, and I. Collings, "New properties of complex noncentral quadratic forms and bounds on MIMO mutual information," in *Proc. IEEE Int. Symp. Inf. Theory*, Seattle, WA, USA, Jul. 2006, pp. 1209–1213.
- [36] T. M. Cover and J. A. Thomas, *Elements of Information Theory*. Hoboken, NJ, USA: Wiley, 1991.
- [37] H. Q. Ngo, E. G. Larsson, and T. L. Marzetta, "Energy and spectral efficiency of very large multiuser MIMO systems," *IEEE Trans. Commun.*, vol. 61, no. 4, pp. 1436–1449, Apr. 2013.
- [38] X. Hong, Y. Jie, C.-X. Wang, J. Shi, and X. Ge, "Energy-spectral efficiency trade-Off in virtual MIMO cellular systems," *IEEE J. Sel. Areas Commun.*, vol. 31, no. 10, pp. 2128–2140, Oct. 2013.
- [39] I. Ku, C.-X. Wang, and J. Thompson, "Spectral, energy and economic efficiency of relay-aided cellular networks," *IET Commun.*, vol. 7, no. 14, pp. 1476–1486, Sep. 2013.
- [40] S. Tombaz, A. Vastberg, and J. Zander, "Energy- and cost-efficient ultra-high-capacity wireless access," *IEEE Trans. Wireless Commun.*, vol. 18, no. 5, pp. 18–24, Oct. 2011.
- [41] B. Lee and S.-L. Kim, "Characterizing energy and deployment efficiency relations in cellular systems," in *Proc. IEEE ICSPCS*, Gold Coast, QLD, Australia, Dec. 2012, pp. 1–5.
- [42] J. Akhtman and L. Hanzo, "Power versus bandwidth-efficiency in wireless communications: The economic perspective," in *Proc. IEEE VTC-Fall*, Anchorage, AK, USA, Sep. 2009, pp. 1–5.
- [43] E. Björnson, L. Sanguinetti, J. Hoydis, and M. Debbah, "Designing multi-user MIMO for energy efficiency: When is massive MIMO the answer?" in *Proc. IEEE WCNC*, Istanbul, Turkey, Apr. 2014, pp. 242–247.
- [44] "Quarterly energy prices," Dept. Energy Climate Change, London, U.K., Tech. Rep. 14D/276C, Sep. 2014. [Online]. Available: https://www.gov.uk/government/uploads/system/uploads/attachment_data/file/368077/qep_Sep_14.pdf
- [45] "Communications market report," Ofcom, London, U.K., Tech. Rep. 2014_UK_cmr, Aug. 2014. [Online]. Available: http://stakeholders.ofcom.org.uk/binaries/research/cmr/cmr14/2014_UK_CMR.pdf



Piya Patcharamaneepakorn received the B.Eng. degree in electrical engineering from Chulalongkorn University, Bangkok, Thailand, in 1999, the M.Eng. degree in telecommunications from the Asian Institute of Technology, Pathum Thani, Thailand, in 2001, and the Ph.D. degree in electrical and electronics engineering from the University of Bristol, Bristol, U.K., in 2014. From 2002 to 2009, he was an RF Optimization Engineer with several companies, including TA-Orange Thailand, T-Mobile Netherlands, and Nokia Siemens Network Argentina. From

2014 to 2015, he was a Post-Doctoral Research Associate with Heriot-Watt University, Edinburgh, U.K. He is currently an Engineering Expert with True Corporation, Bangkok. His research interests include 5G communications systems, multi-user multiple-input multiple-output (MU-MIMO) precoding designs, and massive MIMO systems.



Cheng-Xiang Wang (S'01–M'05–SM'08–F'17) received the B.Sc. and M.Eng. degrees in communication and information systems from Shandong University, China, in 1997 and 2000, respectively, and the Ph.D. degree in wireless communications from Aalborg University, Denmark, in 2004.

He was a Research Fellow with the University of Agder, Kristiansand, Norway, from 2001 to 2005, a Visiting Researcher with Siemens AG Mobile Phones, Munich, Germany, in 2004, and a Research Assistant with the Hamburg University of Technology, Hamburg, Germany, from 2000 to 2001. He has been with Heriot-Watt University, Edinburgh, U.K., since 2005, where he was promoted to a Professor in 2011. He is also an Honorary Fellow with The University of Edinburgh, U.K., and a Chair/Guest Professor with Shandong University and Southeast University, China. He has authored two books, a book chapter, and over 300 papers in refereed journals and conference proceedings. His current research interests include wireless channel modeling and (B)5G wireless communication networks, including green communications, cognitive radio networks, high mobility communication networks, massive MIMO, millimetre wave communications, and visible light communications.

Prof. Wang is a fellow of the IET and HEA, and a member of the EPSRC Peer-Review College. He received nine best paper awards from the IEEE Globecom 2010, the IEEE ICCT 2011, the ITST 2012, the IEEE VTC 2013, IWCMC 2015, IWCMC 2016, the IEEE/CIC ICC 2016, and the WPMC 2016. He is serving or served as a TPC member, the TPC chair, and the general chair of over 80 international conferences. He served or is currently serving as an Editor for nine international journals, including the IEEE TRANSACTIONS ON VEHICULAR TECHNOLOGY since 2011, the IEEE TRANSACTIONS ON COMMUNICATIONS since 2015, and the IEEE TRANSACTIONS ON WIRELESS COMMUNICATIONS from 2007 to 2009. He was a leading Guest Editor of the IEEE JOURNAL ON SELECTED AREAS IN COMMUNICATIONS, Special Issue on Vehicular Communications and Networks. He is also a Guest Editor of the IEEE JOURNAL ON SELECTED AREAS IN COMMUNICATIONS, Special Issue on Spectrum and Energy Efficient Design of Wireless Communication Networks and Special Issue on Airborne Communication Networks, and the IEEE TRANSACTIONS ON BIG DATA, Special Issue on Wireless Big Data. He is recognized as a Web of Science 2017 Highly Cited Researcher.



Yu Fu received the B.Sc. degree in computer science from Huaqiao University, Quanzhou, China, in 2009, the M.Sc. degree in information technology (mobile communications) and the Ph.D. degree in wireless communications from Heriot-Watt University, Edinburgh, U.K., in 2010 and 2015, respectively.

He has been a Post-Doctoral Research Associate with Heriot-Watt University, since 2015. His main research interests include advanced MIMO communication technologies, wireless channel modeling and simulation, RF tests, and software defined networks.



El-Hadi M. Aggoune (M'83–SM'93) received the M.S. and Ph.D. degrees in electrical engineering from the University of Washington (UW), Seattle, WA, USA. He taught graduate and undergraduate courses in electrical engineering at many universities in USA and abroad. He served at many academic ranks, including an endowed chair professor. He is a Professional Engineer registered in the State of Washington. He is currently a Professor and the Director of the SNCS Research Center, University of Tabuk. He has authored many papers in the IEEE

and other journals and conferences. He is listed as an Inventor in two patents assigned to the Boeing Company, USA, and the Sensor Networks and Cellular Systems Research Center, University of Tabuk, Saudi Arabia. His research is referred to in many patents, including patents assigned to ABB, Switzerland, and EPRI, USA. His research interests include wireless sensor networks, energy systems, and scientific visualization. He is serving on many technical committees for conferences worldwide as well as reviewer for many journals. One of his Laboratories received the Boeing Supplier Excellence Award. He received the IEEE Professor of the Year Award, UW Branch.



Mohammed M. Alwakeel (SM'14) was born in Tabuk, Saudi Arabia. He received the B.S. and M.S. degrees from King Saud University, Riyadh, Saudi Arabia, and the Ph.D. degree in electrical engineering from Florida Atlantic University, Boca Raton, Florida. He was a Communications Network Manager with the Saudi National Information Center, Riyadh. He was a Faculty Member with King Abdulaziz University and then an Associate Professor and the Dean of the Computers and Information Technology College, University of Tabuk, Tabuk.

After that, he was a Full Professor with the Computers and Information Technology College, and the Vice Rector for development and quality with the University of Tabuk. He is currently a member of the Alshura Council (The Consultative Council of the Kingdom of Saudi Arabia). His current research interests include teletraffic analysis, mobile satellite communications, and sensor networks and cellular systems.



Xiaofeng Tao (SM'13) received the B.S. degree in electrical engineering from Xi'an Jiaotong University, Xi'an, China, in 1993, and the M.S.E.E. and Ph.D. degrees in telecommunication engineering from the Beijing University of Posts and Telecommunications (BUPT), Beijing, China, in 1999 and 2002, respectively. He is currently a Professor with BUPT, and the Chair of the IEEE ComSoc Beijing Chapter. He has authored or co-authored of 160 papers and three books, in wireless communication areas. He was an inventor or co-inventor of

74 patents. His current research focuses on 5G research. He is a fellow of the IET.



Xiaohu Ge (M'09–SM'11) received the Ph.D. degree in communication and information engineering from the Huazhong University of Science and Technology (HUST) in 2003. He was a Researcher with Ajou University, South Korea, and Politecnico Di Torino, Italy, from 2004 to 2005. He is currently a Full Professor with the School of Electronic Information and Communications, HUST, China. He is also an Adjunct Professor with the Faculty of Engineering and Information Technology, University of Technology Sydney, Australia. He has published

about 160 papers in refereed journals and conference proceedings, and has been holding about 15 patents in China. His research interests are in the area of mobile communications, traffic modeling in wireless networks, green communications, and interference modeling in wireless communications. He is a Senior Member of the China Institute of Communications, and a member of the National Natural Science Foundation of China and the Chinese Ministry of Science and Technology Peer-Review College. He has been actively involved in organizing over the ten international conferences, since 2005. He served as the General Chair for the 2015 IEEE International Conference on Green Computing and Communications (the IEEE GreenCom). He serves as an Associate Editor for the IEEE TRANSACTIONS ON VEHICULAR TECHNOLOGY and the IEEE WIRELESS COMMUNICATIONS.